Sensitivity Studies of Four-Dimensional Local Ensemble Transform Kalman Filter Coupled With WRF-Chem Version 3.9.1 for Improving Particulate Matter Simulation Accuracy

Jianyu Lin[1,2], Tie Dai[2*], Lifang Sheng[1], Weihang Zhang[1], Shangfei Hai[3], Yawen Kong[4]

[1] College of Oceanic and Atmospheric Sciences, Ocean University of China, Qingdao, 266100, China

[2] State Key Laboratory of Numerical Modeling for Atmospheric Sciences and Geophysical Fluid Dynamics, Institute of Atmospheric Physics, Chinese Academy of Sciences, Beijing, China

[3] CMA Earth System Modeling and Prediction Centre, China Meteorological Administration (CMA), Beijing 100081

[4] State Key Laboratory of Remote Sensing Science, Aerospace Information Research Institute, Chinese Academy of Sciences, Beijing 100101, China

Correspondence:Tie Dai (daitie@mail.iap.ac.cn)

Abstract: Accurately simulate severe haze events through numerical models remains challenging because of uncertainty in anthropogenic emissions and physical parameterizations of particulate matter ($PM_{2.5}$ and PM_{10}). In this study, a coupled WRF-Chem/four-dimension local ensemble transform Kalman filter (4D-LETKF) data assimilation system has been successfully developed to optimize particulate matter concentration by assimilating hourly

带格式的: 字体颜色: 红色

ground-based observations in winter over the Beijing-Tianjin-Hebei region and surrounding provinces. The effectiveness of 4D-LETKF system and its sensitivity to ensemble member size and length of assimilation window have been investigated. The promising results show that significant improvements have been made by analysis in the simulation of particulate matter during severe haze event. The assimilation reduces root mean square errors of $PM_{2.5}$ from 69.93 to 31.19 μg m^{-3} and of PM_{10} from 106.88 to 76.83μg m^{-3}. Smaller RMSEs and larger correlation coefficients in the analysis of $PM_{2.5}$ and PM_{10} are observed across nearly all verification stations, indicating that the 4D-LETKF assimilation optimizes the simulation of $PM_{2.5}$ and PM_{10} concentration efficiently. Sensitivity experiments reveal that the combination of 48 hours of assimilation window length and 40 ensemble members shows best performance for reproducing severe haze event. In view of the performance of ensemble members, increasing ensemble member size improves ~~divergence~~ ensemble spread among each forecasting member, facilitates the spread of state vectors about $PM_{2.5}$ and PM_{10} information in the first guess, favors the variances between each initial condition in the next assimilation cycle and leads to better simulation performance both in severe and moderate haze events. This study advances our understanding about the selection of basic parameters in the 4D-LETKF assimilation system and the performance of ensemble simulation in a particulate matter polluted environment.

Key words: 4D-LETKF, severe haze simulation, ensemble member size, length of assimilation window

带格式的: 字体颜色: 红色

1. Introduction

Although great progress about air pollution control has been made during recent years,

China is facing the highest levels of particulate matter in the world (van Donkelaar et al., 2016). Particulate matter consists of $PM_{2.5}$ and PM_{10}, refers to particles with aerodynamic diameters of less than 2.5 and 10 μm, respectively. High concentration of particulate matter is a major factor for severe haze events (air quality index larger than 200) in the Beijing-Tianjin-Hebei (BTH) region of China, especially during winter (Yan et al., 2016, Zhang et al., 2018). Numerical models are considered to be useful tools for simulating haze events as for taking complex physical and chemical mechanisms into account, but the uncertainty in emissions and physical parameterizations still remain a significant barrier in improving the simulation accuracy (Gao et al., 2017, Feng et al., 2018).

As an effective statistical approach, data assimilation is capable of improving the accuracy of pollution simulations by limiting the performance of models. Lots of data assimilation approaches have been applied to the atmospheric science, including three-dimension variation (3D-Var) (Lorenc 1986; Parrish and Derber 1992; Sun et al., 2020), four-dimension variation (4D-Var) (Huang et al. 2009; Benedetti et al., 2009), ensemble Kalman filter algorithms and their variants (Evensen 1994; Whitaker and Hamill 2002; Miyazaki et al., 2012a), etc. Among them, four-dimension local ensemble transform Kalman filter (4D-LETKF) has shown unique characteristics in numerical simulation (Evensen, 2003, Kong et al., 2021). Firstly, derived from finite forecasting members, the background error covariance matrix of 4D-LETKF features flow-dependent characteristics, and the linear combinations of ensemble members produce global analysis (Hunt et al., 2007). Secondly, the computational time for 4D-LETKF remains robust as the observation numbers increase, exhibiting strong computational ability in the parallel architecture when assimilate various measurements (Miyoshi et al., 2007; Hunt et al.,

2007, Dai et al., 2021). Lastly, 4D-LETKF can assimilate time slots of asynchronous observations to optimize the current state within the assimilation window, which efficiently improves the quality of pollution prediction (Evensen, 2003, Ott et al., 2004, Dai et al., 2019, Cheng et al., 2019).

The characteristics of 4D-LETKF underscore the importance of ensemble member size and length of assimilation window on its effectiveness. The ensemble member decides the background error covariance matrix, representing the uncertainty in ensemble simulations (Peng et al., 2017). 4D-LETKF considers approximate model trajectories by linear combinations of the background ensemble trajectories. However, limited numbers of ensemble members may bring about insufficient dispersion of ensemble systems (Hunt et al., 2004). In addition, 4D-LETKF system can greatly improves the utilization rate of observations by constrain the state variables in asynchronous hourly slot within the assimilation window. A longer assimilation window efficiently reduces computational load by avoiding frequent switches between state and forecast variables. But the trajectories over a long length of assimilation window may diverge enough that linear combinations will not approximate the model trajectories. Moreover, the model ensemble trajectory may not fit the observations well over the entire interval with the presence of model errors (Dai et al., 2019). Many studies have discussed the choice of these two parameters for ensemble Kalman filter algorithms and their variants. When optimizing hourly aerosol fields by satellite observations, Cheng et al. (2019) revealed that the forecast with a 24-hour assimilation window was comparable to those with 1-hour, the root mean square error for AOD are 0.091 and 0.110, respectively, indicating the weights determined at the end of the 24 hours assimilation window are valid to optimize the

ensemble trajectories. While Dai et al. (2019) proposed that over 80% of the hourly assimilation efficiencies for the 1-hour assimilation window are higher than those with 6- or 24-hours in 4D-LETKF experiments, suggesting that assimilation efficiency decreases with the increase of the assimilation window interval. These different opinions reveal that there is still a large uncertainty about selection of parameters in 4D-LETKF assimilation system.

The accuracy simulation of severe haze events with air quality index (AQI) larger than 200 has been a challenging problem for a long time, posing severe threats to human daily life and public health (Wang et al., 2014, Kong et al., 2021, Gao et al., 2017). Although 4D-LETKF has unique advantages in computational efficiency and analysis, there are few researches investigate the impacts of 4D-LETKF assimilation on pollutant simulation especially in severe haze events, in addition, it is also imperative to explore the basic optimal combination of assimilation parameters and its explanation in this method. Our major objectives are not only to evaluate the performance of 4D-LETKF in reproducing particulate matter concentration during severe haze event, but also to summarize the influence rules of ensemble size and assimilation window length on particulate matter simulation, and explore whether these rules are applicable to moderate haze event (air quality index smaller than 200) as well. The results have great significance to verify and quantify the effect of 4D-LETKF assimilation on numerical simulations of $PM_{2.5}$ and PM_{10}, subsequently providinge a general rule for parameter selection in the 4D-LETKF during severe haze events. Herein, we utilize 4D-LETKF system which was coupled with Weather Research and Forecasting with Chemistry (WRF-Chem) model to improve simulative skill of particulate matter among northern China during the winter of 2020. Section 2 briefly introduces detail setting of WRF-Chem model, 4D-LETKF,

带格式的: 字体颜色: 红色

带格式的: 字体颜色: 红色

observations and numerical experiment designs. Section 3 compares the assimilation with those in the prior simulation, summarizes and explains sensitivity rules for parametric selection, and followed by a conclusion in Section 4 lastly.

2. Methodology

2.1 Configuration of the forecast model

In our implementation, the fully coupled "online" WRF-Chem version 3.9.1 is employed as numeral forward model to describe the meteorological and chemical conditions simultaneously, which fully considers extensive chemical transport processes including advection, convection and sedimentation processes (Grell et al., 2005). The WRF-Chem model is configured with two domains (d01 and d02), both using 100 (west–east) ×100 (south–north) grid points, but with horizontal resolutions of 30 and 10 km, respectively. As shown in Figure 1(a), the d01 domain covers most part of East Asia, and the area under the blue shadow is the d02 domain. The vertical grid contains 40 full sigma levels, extending from the surface to 50 hPa.

The initial and lateral boundary conditions of meteorological fields are derived from the National Centers for Environmental Prediction Final (FNL) analysis data with a spatial resolution of 1°×1° and temporal interval of 6 hours. A state-of-the-art and highly non-linear gas-phase chemical mechanism Regional Atmospheric Chemistry Mechanism (RACM) (Stockwell et al., 1997) is selected as gas phase mechanism, and Goddard Chemistry Aerosol Radiation and Transport (GOCART) (Schwartz et al., 2012) is adopted as aerosol mechanism. The parameterization scheme used in research is shown in Table 1.

Table 1. WRF-Chem parameterization scheme in this study.

Parameterization	WRF-Chem option
Microphysics	Morrison 2–moment Scheme (Morrison et al., 2019)
Longwave radiation	RRTMG Longwave Scheme (Iacono et al., 2008)
Shortwave radiation	RRTMG Shortwave Scheme (Iacono et al., 2008)
Planetary boundary layer	YSU Scheme (Hong et al., 2006)
Cumulus parameterization	Grell 3D Ensemble Scheme (Grell et al., 1993)
Land surface model	Noah (Tewari et al., 2004)

The anthropogenic emissions are obtained from the Multi-resolution Emission Inventory for China compiled by Tsinghua University (MEIC, http://www.meicmodel.org/). The inventory includes anthropogenic emissions from agriculture, industry, power, residential and transportation sectors (Zheng et al., 2021). Inventory with a spatial resolution of 0.25°×0.25° and has been interpolated to match the simulation resolution. The biogenic emissions are calculated online by Guenther scheme (Guenther et al. 1995). The $PM_{2.5}$, PM_{10} concentrations output from WRF-Chem are linearly interpolated to site observations. The evaluation of uncertainty in the emission inventory has been shown in previous research (Zhang et al., 2009).

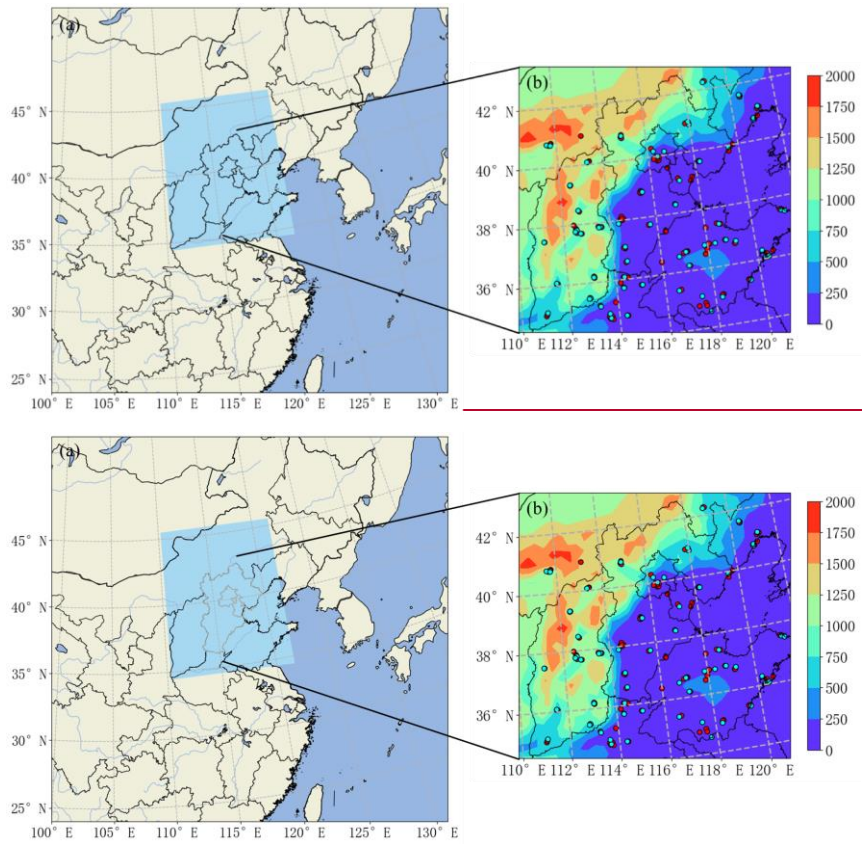

Figure 1. (a) WRF-Chem model domains. The grey border implies the BTH region. (b) Location of assimilated and independent verification observation sites with topography (units: m). The red and blue dot implies the assimilated and independent verification observation site, respectively.

带格式的: 字体颜色: 红色

2.2 The 4D-LETKF algorithm and the state variables

The 4D-LETKF coupled with WRF-Chem Model is implemented to investigate the influence of assimilation on particulate matter simulation in this research. In this section, we introduce the 4D-LETKF algorithm and corresponding state variables briefly, more detailed information can be found in Hunt et al. (2007). The LETKF features a flow-dependent

covariance matrix from ensemble simulation and determines the analysis ensemble mean $\overline{x^a}$ (a posteriori) according to the following formula:

$$\bar{x}^a = \bar{x}^b + X^b \bar{w}^a$$

where $\bar{x}^b$ and X^b denote ensemble mean of first guess and background ensemble perturbations, respectively. The ensemble perturbation matrix X^b is calculated as $x^b(i) - \bar{x}^b$ ~~$x(i) - \bar{x}$~~, $\{i = 1, 2, ..., k\}$, which k represents the ensemble member size. The perturbation weight matrix $\bar{w}^a$ is the Kalman gain which linearly determines the increment between the analysis and the first guess, and can be calculated as:

$$\bar{w}^a = \widetilde{P^a}\left(Y^b\right)^T R^{-1}(y^0 - \bar{y}^b)$$

where $\widetilde{P^a}$ is analysis error covariance in ensemble space. y^0 and $\bar{y}^b$ denote the observations vector and ensemble mean background observations, respectively. Ensemble mean background observations derived from applying observation vector to ensemble member state vector H ($\bar{x}^b$). The matrix R is the observation error covariance matrix. The matrix Y^b represents ensemble background observation perturbations, whose i th columns is $y^{b(i)}(i) - \bar{y}^b$, $\{i = 1, 2, ..., k\}$. $\widetilde{P^a}$ can be obtained as:

$$\widetilde{P^a} = [(k-1)I/\rho + (Y^b)^T R^{-1} Y^b]^{-1}$$

where I denotes the identity matrix and k is ensemble member size. To prevent from filter divergence, the multiplicative inflation factor ρ is set to 1.1 to inflate the analysis covariance (Dai et al., 2019, Anderson, 2007). Analysis ensemble perturbations X^a is calculated by:

$$X^a = X^b \left[(k-1)\widetilde{P^a}\right]^{1/2} = X^b W^a$$

Calculated by the sum of the $\bar{x}^a$ and each of the columns of ~~X^a~~, the ensemble analyses are served as optimal initial conditions in each ensemble member to generate the first guess in

带格式的: 字体颜色: 红色, 上标
带格式的: 字体颜色: 红色
带格式的: 字体颜色: 红色
带格式的: 字体颜色: 红色
带格式的: 字体颜色: 红色
带格式的: 字体颜色: 红色
带格式的: 字体颜色: 红色
带格式的: 字体颜色: 红色
带格式的: 字体颜色: 红色
带格式的: 字体颜色: 红色
带格式的: 字体颜色: 红色
带格式的: 字体颜色: 红色
带格式的: 字体颜色: 红色
带格式的: 字体颜色: 红色
带格式的: 字体颜色: 红色
带格式的: 字体颜色: 红色
带格式的: 字体颜色: 红色
带格式的: 字体颜色: 红色
带格式的: 字体颜色: 红色
带格式的: 字体颜色: 红色

the next cycle.

Figure 2 is the flow chart of the WRF-Chem/4D-LETKF assimilation system applied in our implementation. The system conducts these processes within each assimilation cycle. The 4D-LETKF generates a flow-dependent background error covariance matrix by ensemble member. Given that the emissions inventory is an important source of uncertainty in simulation (Pagowski and Grell, 2012), the research randomly perturbs anthropogenic emissions of PM, black carbon (BC) and organic carbon (OC) in January for each member to create the ensemble members, and the perturbation follows a log-normal distribution in the k-dimensional space. The mean values of perturbations of $PM_{2.5}$, PM_{10}, BC and OC emissions are equal to 1, and the variances of these emissions are set according to corresponding uncertainty in MEIC inventory (130%, 132%, 208%, 258% for $PM_{2.5}$, PM_{10}, BC, OC, respectively) (Luo et al., 2023). Such ensemble anthropogenic emissions are perfect correlation in spatial and temporal dimension and should not be regarded as overly restrictive (Schutgens et al., 2010). This study only adds one times of perturbations into emissions at the first cycle of assimilation to provide the information spread of particulate matter. It is enough to make most of the site information affect the first-guess field. The WRF-Chem/4D-LETKF system propagates the ensemble forward simulation for the entire assimilation window time and outputs the first guess fields at each hourly time slot. The ensemble mean of first guess ($\bar{x}^b$) and background ensemble perturbations (X^b) can be obtained from ensemble member here. Combining observation and observation operator, the innovation ($y^0 - \bar{y}^b$) and Y^b can be obtained in each time slot. The perturbation weight matrix $\bar{w}^a$ is valid within a relative short assimilation window (e.g., 24 or 48 hours) (Hunt et al., 2004, Cheng et al., 2019). The analysis ensemble derived from $\bar{w}^a$ at the end of

带格式的: 字体颜色: 红色
带格式的: 字体颜色: 红色, 下标
带格式的: 字体颜色: 红色
带格式的: 字体颜色: 红色, 下标
带格式的: 字体颜色: 红色
带格式的: 字体颜色: 红色

time slots will serve as chemical initial conditions for the next assimilation window. As the cycle of assimilation proceed, a linear combination of analysis ensemble is continuously obtained.

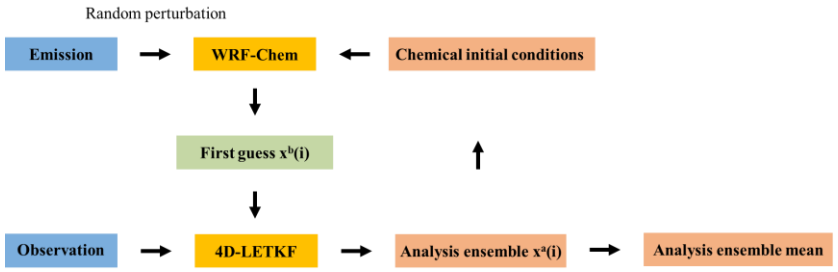

Figure 2. Flow chart of the WRF-Chem/4D-LETKF assimilation system for particulate matter.

The ensemble Kalman filter generally encounters a spurious long-distance correlation problem because of the limited numbers of ensemble members (Miyazaki et al., 2012a). To avoid the problem above, it is necessary to apply observation localizations to filter observation from a long distance. 4D-LETKF offers a flexible choice of observation localizations in horizontal, vertical and temporal dimensions for each grid point (Cheng et al., 2019). In this study, the horizontal localization factor is calculated as Gaussian function (Miyoshi et al., 2007), which gradually reduces the effect of observation as the increasing departure from the analysis grid:

$$f(r) = \exp(-r^2/2\sigma^2)$$

Here, r represents physical distance from observation to analysis grid and σ represents localization length. We limit the localization factor from 0 to 3.65 times the localization length (Zhao et al., 2015), ignoring the observation beyond 3.65 times the localization length to the analysis grid.

The selection of the state variables depends on the generative mechanism of aerosol. As a result, 16 kinds of WRF-Chem/GOCART aerosol variables are treated as state variables. For the $PM_{2.5}$ observations, the observation operator is described as:

$$y^{bf}_{PM_{2.5}} = \rho_d[P_{2.5} + 1.375\mathrm{S} + 1.8(OC_1 + OC_2)$$

$$+BC_1 + BC_2 + D_1 + 0.286D_2 + S_1 + 0.942S_2]$$

where ρ_d present the dry-air density, $P_{2.5}$ is the fine unspecified aerosol contributions, S represents sulfate, OC_1 and OC_2 are hydrophobic and hydrophilic organic carbon, respectively. BC_1 and BC_2 are hydrophobic and hydrophilic black carbon, D_1 and D_2 are dusts with effective radii of 0.5 and 1.4 μm, and S_1 and S_2 are sea salts with effective radii of 0.3 and 1.0 μm, respectively (Peng et al., 2018).

Similarly, the observation operator for PM_{10} is shown as below:

$$y^{bf}_{PM_{10}} = \rho_d[P_{10} + P_{2.5} + 1.375\mathrm{S} + 1.8(OC_1 + OC_2)$$

$$+BC_1 + BC_2 + D_1 + 0.286D_2 + D_3 + 0.87D_4 + S_1 + 0.942S_2 + S_3]$$

where P_{10} is coarse unspecified aerosol contributions, D_3 and D_4 are dusts with effective radii of 2.4 and 4.5 μm. S_3 is sea salt with effective radii of 3.2 μm. Therefore, the simulated $PM_{10\text{-}2.5}$ is:

$$y^{bf}_{PM_{10-2.5}} = \rho_d[P_{10} + D_3 + 0.87D_4 + S_3]$$

In this research, $y^o_{PM_{10-2.5}}$ calculated by $y^o_{PM_{10}} - y^o_{PM_{2.5}}$ is used to analyze state variables including D_5 and S_4, which are dust with effective radii of 8 μm and sea salt with effective radii of 7.5 μm, respectively.

2.3 Site observation data and errors

Ground-based observation features high temporal resolution, which can capture variation

带格式的: 字体颜色: 红色

带格式的: 字体颜色: 红色

带格式的: 字体颜色: 红色

of pollution concentration on an hourly scale at the bottom of the troposphere, providing continuous and reliable observation. The quality-assure and quality-controlled hourly observation data of $PM_{2.5}$ and PM_{10} are used to explore the influence of 4D-LETKF assimilation in this research. The pollution data was obtained from China National Environmental Monitoring Center (http://106.37.208.233:20035/). As the research primarily focuses on the BTH region, the assimilation and verification sites are mainly located in the BTH region and neighboring provinces, primarily located in urban and suburban areas. In order to obtain more reliable observation data, the quality control of observation data in this study includes hourly observation of default value and extreme value detection. First, during the haze period, if the number of missing values for either type of pollutant at one site exceeds 24 hours, this site is considered to have a certain uncertainty on observation quality, and data will not be assimilated. Second, for each kind of observation in different station, the hourly observation outside the range of $m \pm 3\sigma$ will not be assimilated, where the m and σ denote the mean value and standard deviation of daily time series, respectively. When selecting assimilation and verification sites, spatial distribution uniformity is ensured for better assimilation performance, consequently, those sites are randomly selected. Finally, 127 assimilation sites and 69 verification sites in the BTH region and surrounding province are selected (Figure 1b). It can be seen that the assimilation and verification sites have a relatively uniform spatial distribution.

The observation error covariance matrix (R) is assumed to be diagonal, implying that observational errors among each pollution species are uncorrelated. The observation error (r) consists of measurement error (ε_0) and representation error (ε_r):

$$r = \sqrt{\varepsilon_0^2 + \varepsilon_r^2}$$

The measurement error ε_0 is defined as:

$$\varepsilon_0=\text{ermax}+0.0075*\Pi_0$$

where ermax is the base error, which is set to be 1 for $PM_{2.5}$, and PM_{10} (Chen et al., 2019a), Π_0 denotes the observation of concentration. Produced by observation operator, representativeness errors can be calculated by the formula (Elbern et al., 2007):

$$\varepsilon_r=\gamma\,\varepsilon_0\sqrt{\Delta l/L}$$

γ is tunable scaling factor and 0.5 is set for γ, Δl is the spatial resolution of gridding (30 km and 10km for d01 and d02, respectively), L depends on station location, which denotes the range that an observation can reflect, here L is 2 km for calculation.

Meteorological data were collected from National Climatic Data Center (https://wwww.ncei.noaa.gov/), which provides hourly air temperature, dew point, and windspeed data. The observational meteorological data are used to validate the performance of simulations in this study.

2.4 Experiment design

A series of control and data assimilation experiments during severe and moderate haze events, as listed in Table 2, have been carried out to achieve our major objective. The control experiments refer to numerical experiments without data assimilation. The Severe-FR experiment with 48 hours spin up time is performed firstly to quantify the necessity of adjusting particulate matter concentration during severe haze event. Severe-FR-24h, Severe-FR-48h, and Severe-FR-72h accompany with restart every 24, 48, and 72 hours respectively and update meteorological boundary conditions. Except Severe-FR, the rest of the experiments all have 24 hours of spin up time at the beginning of each restart or assimilation cycle. The settings of

带格式的: 字体: 倾斜, 字体颜色: 红色

带格式的: 字体: 倾斜, 字体颜色: 红色

带格式的: 字体: 倾斜, 字体颜色: 红色

带格式的: 字体颜色: 红色

assimilation experiments cycle time are same with corresponding control experiments. The detail descriptions of experiment cycle time are shown in Figure S1. Since the effectiveness of 4D-LETKF is highly related with ensemble member size and length of assimilation window (Rubin et al., 2016), the sensitivity analysis is employed to investigate the influence from two parameters on assimilation effect (Kong et al., 2023). The selection of assimilation parameters for the sensitivity experiments includes 20, 40 and 60 for ensemble members, and 24, 48 and 72 hours for the length of assimilation window empirically (Kong et al., 2021, Dai et al., 2021). All sensitivity experiments use identical WRF-Chem physical parameterizations, anthropogenic emission and random perturbations. Through the comparison between all assimilation experiments, the influence rules of 4D-LETKF assimilation on the simulation of particulate matter in severe haze can be retrieved. Lastly, aiming to determinate the applicable range of obtained influence rules above, two assimilation experiments in a moderate haze event are performed to validate whether the rules are also suitable to a less-polluted environment. The detail reasons for selection of parameters will be fully described in the next section.

Table 2. design of numerical experiments in this research.

	Experiment	Design of simulation
Control experiments	Severe-FR	Free run experiment in severe haze event and without restart in integration process.
	Severe-FR-24h Severe-FR-48h Severe-FR-72h	Free run experiment in severe haze event and with restart every 24, 48 and 72 hours, provide deterministic simulation corresponding to data assimilation experiment.

	Moderate-FR-48h	Free run experiment in moderate haze events and with restart every 48 hours, provide deterministic simulation corresponding to data assimilation experiment.
Data assimilation experiments in severe haze event	Severe-20m-24h Severe-20m-48h Severe-20m-72h	Assimilation experiment in severe haze event with 20 ensemble members and 24, 48, 72 hours of assimilation window length respectively.
	Severe-40m-24h Severe-40m-48h Severe-40m-72h	Assimilation experiment in severe haze event with 40 ensemble members and 24, 48, 72 hours of assimilation window length respectively.
	Severe-60m-24h Severe-60m-48h Severe-60m-72h	Assimilation experiment in severe haze event with 60 ensemble members and 24, 48, 72 hours of assimilation window length respectively.
Data assimilation experiments in moderate haze event	Moderate-20m-48h Moderate-40m-48h	Assimilation experiment in moderate haze event with 20 and 40 ensemble members combine with 48 hours of assimilation window length.

Root mean square error (RMSE), mean errors (BIAS), mean absolute error (MAE) and correlation coefficient are calculated in this study to evaluate the performance of each numerical experiment. The assimilation efficiency (AE) for estimating the data assimilation performance is also calculated from the formulation below (Yumimoto and Takemura, 2011):

$$\mathrm{AE} = \frac{RMSE^{f} - RMSE^{a}}{RMSE^{f}} \times 100\%$$

where $RMSE^{af}$ and $RMSE^{fa}$ is RMSE with and without assimilation, respectively. According to the definition, if AE is positive, it means that RMSE has decreased due to assimilation effect. When AE is equal to 1, RMSE in analysis completely disappears, and analysis is equal to observation. The formulations of correlation coefficient and root mean square error are shown in supplement.

3. Results

3.1 Comparison of the analysis with control experiment

3.1.1 The reproduction ~~simulation~~ of the severe haze event in BTH

It is essential to discuss the basic evolution of pollutant and the necessity of pollutant data assimilation in severe haze event before conducting the assimilation experiments. The severe haze event selected in this study occurred from 00:00 UTC 15 January 2020 to 00:00 UTC 21. The AQI is a comprehensive indictor of overall air pollution and criterion for severe haze events (Zhan et al., 2018, Bao et al., 2015). As a result, Figure 3(a) shows the temporal variation of AQI~~air quality index~~ at the six sites among BTH region during the investigated period. The peak value of AQI mainly appeared on 18 January, and then rapidly decreased on 19 and 20 January. The temporal averaged of AQI have exceeded 200, with particulate matter identified as the primary pollutant. Fig. 3(b) provides the correlation coefficients and standardized standard deviations of five parameters from Severe-FR against observations. Meteorological variables including air temperature, dew point temperature and wind speed are well simulated when compared with $PM_{2.5}$ and PM_{10}. The correlation coefficients of meteorological factors are all larger than 0.6, while that of pollutant concentrations are all below 0.4. Therefore, when the

带格式的: 字体颜色: 红色
带格式的: 字体颜色: 红色
带格式的: 字体颜色: 红色
带格式的: 字体颜色: 红色
带格式的: 字体颜色: 红色
带格式的: 字体颜色: 红色
带格式的: 字体颜色: 红色
带格式的: 字体颜色: 红色

meteorological conditions can be retrieved relatively accurately, particulate matter assimilation is the key to improving the simulative skill of pollutants.

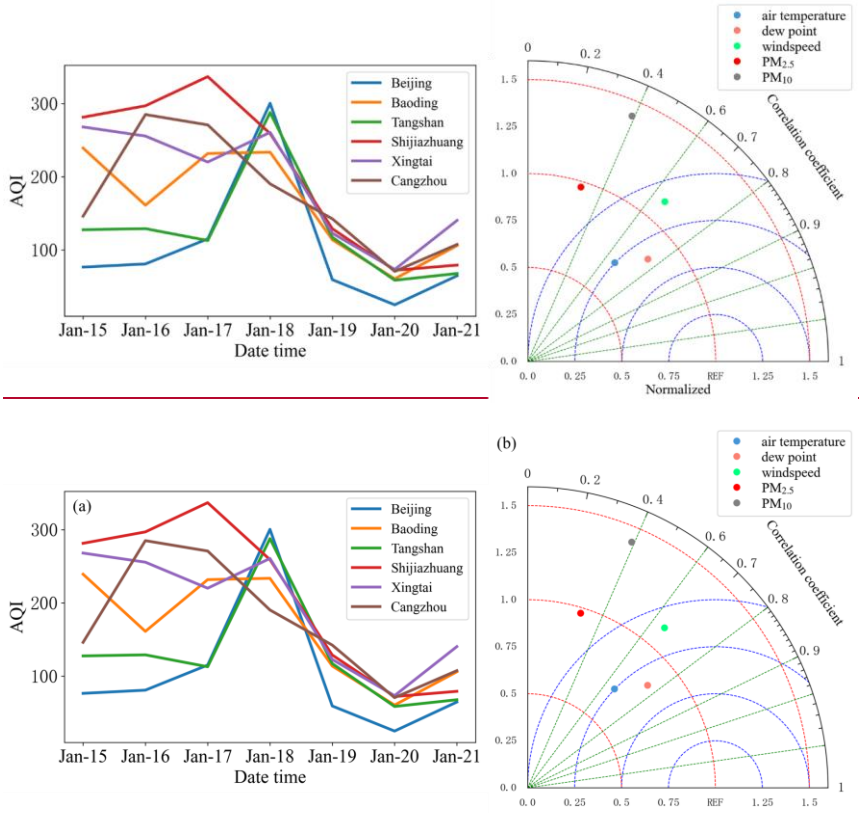

Figure3. (a) Temporal variation about AQI~~air quality index~~ at six sites in severe haze event. (b) A Taylor graph describing simulation from Severe-FR about five kinds of parameters compared with the observed ones in BTH region.

带格式的: 字体颜色: 红色

3.1.2 The improvement ~~of the~~ in the reproduction of severe haze ~~simulation~~ achieved by 4D-LETKF

带格式的: 字体颜色: 红色

The divergence between assimilation and control experiment reflects the contribution from 4D-LETKF initial condition adjustment. Consequently, the study takes an ensemble member

带格式的: 字体颜色: 红色

size of 40 and assimilation window length of 48 hours to conduct sensitivity experiment and compare with Severe-FR-48h which has the same integration time in each cycle to validate the effectiveness of 4D-LETKF assimilation system (the analysis from the selection of 40 ensemble members and 48 hours of assimilation window length is presented here because it shows the best performance among sensitivity experiments in the next section). Figure 4 reveals the performance of control and assimilation experiments in severe haze event. The RMSE values of $PM_{2.5}$ and PM_{10} in Severe-FR-48h are 69.93 and 106.88μg m^{-3} and both with scattered distribution, indicating substantial uncertainty exist in reproducing this severe haze event. In Severe-40m-48h, the RMSE values of $PM_{2.5}$ and PM_{10} are 31.19 and 76.83μg m^{-3}, decreasing by 55.40% and 28.12% respectively in a high particulate matter concentration environment. The decreased RMSE values also imply that the assimilation system has reached a well-calibrated stage. Not only more points are getting together, but smaller simulation errors for $PM_{2.5}$ and PM_{10} also imply that the Severe-40m-48h outperforms the Severe-FR-48h in this severe haze event.

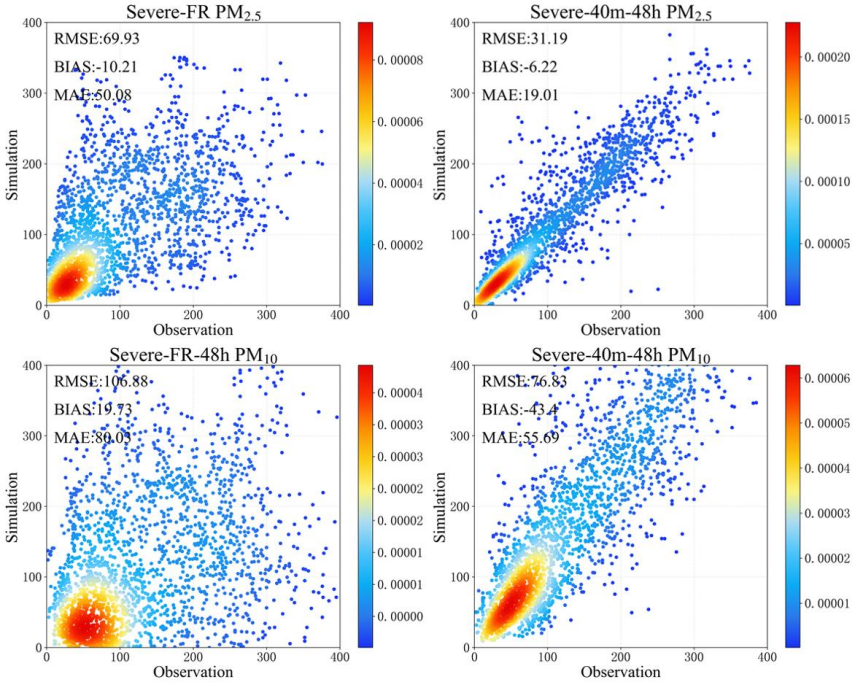

Figure 4. Scatter and density plot of $PM_{2.5}$ and PM_{10} in Severe-FR-48h and Severe-40m-48h versus observations from verification stations (units: μg m^{-3}). The color bar represents the Gaussian Kernel Density estimation.

In order to acquire basis distribution of simulation errors for particulate matter, Figure 5 presents the frequency distribution of deviations between observed and simulated particulate matter concentrations in Sevre-FR-48 and Severe-40m-48h experiments. It is obviously that Severe-40m-48h increases the frequency of low deviations and decrease those of high deviations in the simulation of $PM_{2.5}$. The deviation pattern of $PM_{2.5}$ in Severe-40m-48h is generally squeezed with higher peaking and symmetrical to the value of 0 than Severe-FR-48h. For the deviation distribution pattern of PM_{10}, it shows high frequency of negative deviations and great underestimation in the Severe-FR-48h, and this underestimation has been effectively

带格式的: 字体颜色: 红色

带格式的: 默认段落字体, 字体: (默认) Times New Roman, (中文) 宋体, 11 磅, 字体颜色: 红色, 图案: 清除

带格式的: 字体颜色: 红色

带格式的: 默认段落字体, 字体: (默认) Times New Roman, (中文) 宋体, 11 磅, 字体颜色: 红色, 图案: 清除

带格式的: 字体颜色: 红色

corrected by the adjustment of initial conditions and step analysis in Severe-40m-48h. Specially, the proportion of deviation within 20 μg m^{-3}in the Severe-40m-48h is 69.98% for $PM_{2.5}$ and 31.90% for PM_{10}.

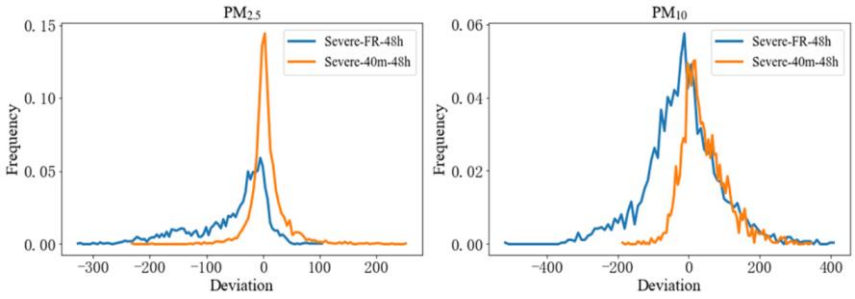

Figure 5. Frequency distribution of the deviations about the simulated $PM_{2.5}$ and PM_{10} concentrations in Severe-40m-48h and Severe-FR-48h minus the observed ones (units for deviation: μg m^{-3}).

带格式的: 字体颜色: 红色

Figure 6 exhibits the spatial distribution of four statistical parameters about RMSE for particulate matter among the BTH region. By comparison from the Severe-FR-48h and Severe-40m-48h, there are significant RMSE reduction for $PM_{2.5}$ after assimilation, implying that the actual evolution of $PM_{2.5}$ can be better represented by Severe-40m-48h. For instance, the RMSE values of $PM_{2.5}$ in Baoding, Hengshui and Cangzhou, have significantly decreased to 29.85, 18.98, and 19.06μg m^{-3}, respectively, compared to 80.55, 55.22 and 76.32 μg m^{-3}in the Severe-FR-48h. AE in most verification stations has exceeded 50% also suggests the high efficiency of 4D-LETKF assimilation for the simulation of $PM_{2.5}$. Although the performance of assimilation experiment in Shijiazhuang city does not have a good agreement with observation and shows a positive difference, high values of AE in most of verification stations also proves the validation of assimilating effect for PM_{10}. Compared to the Severe-FR-48h, the Severe-

40m-48h productively reduces the RMSE of PM_{10}, accompany with high values of 61.18%, 59.17% and 52.18% about AE on Zhangjiakou, Tangshan and Hengshui, respectively.

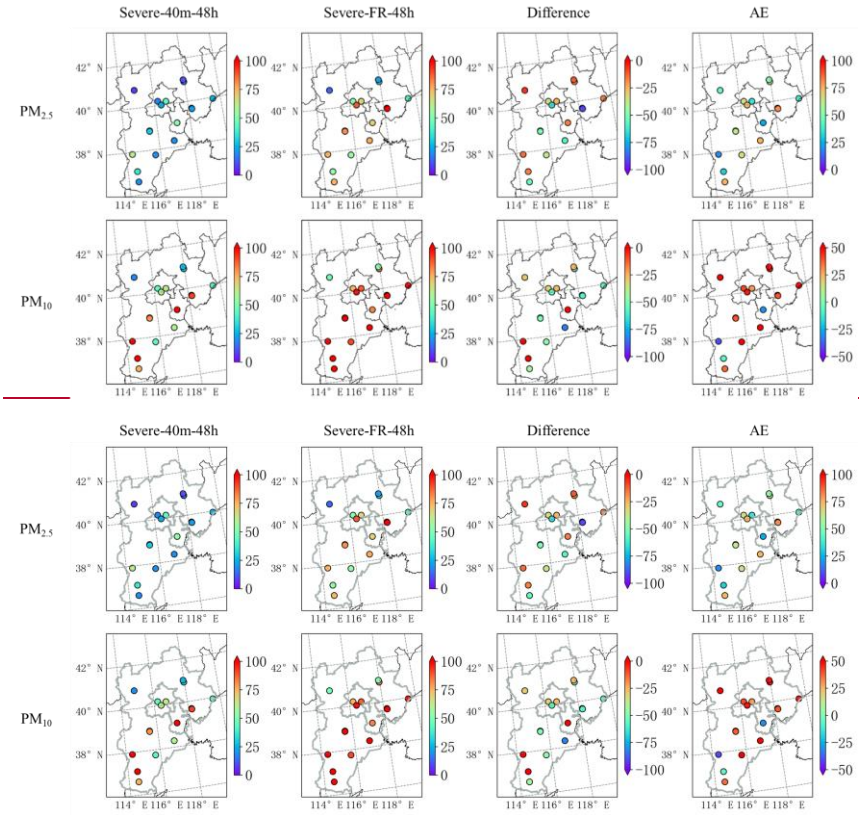

Figure 6. Spatial distribution of RMSE values from Severe-40m-48h (first column), Severe-FR-48h (second column), their difference (third column) and AE (fourth column) for $PM_{2.5}$ (first row) and PM_{10} (second row) from 15 January to 21 January among verification station in BTH region. The difference implies the RMSE in Severe-40m-48h minus those in Severe-FR-48h (units: μg m^{-3}). AE is assimilation efficiency and has been described in methodology before. The grey border implies the BTH region.

The spatial distribution of correlation coefficients from Severe-40m-48h, Severe-FR-48h,

带格式的: 字体颜色: 红色

带格式的: 字体颜色: 红色

their difference for $PM_{2.5}$ and PM_{10} are also illustrated in Figure 7. The assimilation experiment increases the correlation coefficients to more than 0.6 at all sites in the simulations of $PM_{2.5}$ and exceed 0.7 among the southern BTH region in the simulations of PM_{10}. The Severe-40m-48h also reverses the opposite trend of $PM_{2.5}$ and PM_{10} series in Severe-FR-48h versus observations, for example, the correlation coefficients in Severe-FR-48h at Chengde and Zhangjiakou are -0.42 and -0.53, but increase to 0.52 and 0.69 after assimilation in the simulations of PM_{10}. Incorporating more assimilable observations may further increase the correlation coefficient in the simulation of particulate matter (Kong et al., 2021). Data assimilation by multiple observations from diverse platform is necessary because it can integrate and coordinate observational information into aerosol forecasts well and then improve air pollutant forecast accuracy (Barbu et al., 2009, Ma et al., 2020).

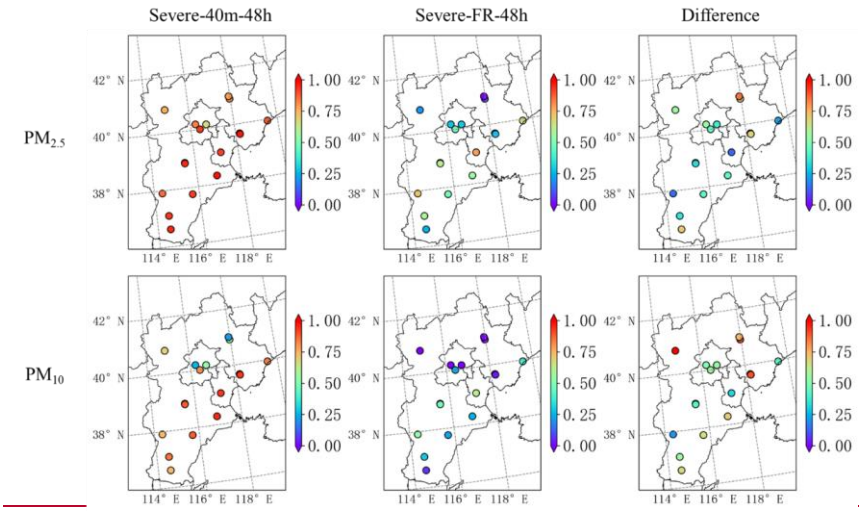

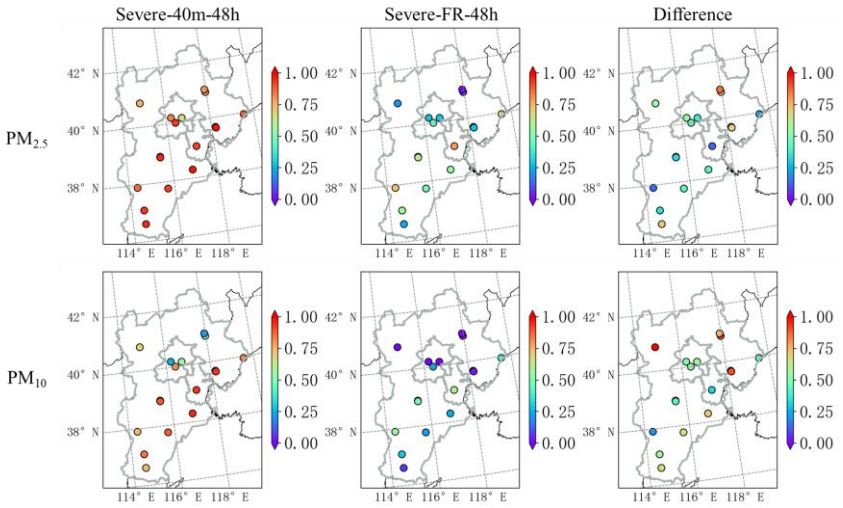

Figure 7. Spatial distribution of correlation coefficients from Severe-40m-48h (first column), Severe-FR-48h (second column), their difference (third column) for $PM_{2.5}$ (first row) and PM_{10} (second row) from 15 January to 21 January among verification station in BTH region. The difference implies the correlation coefficient in Severe-40m-48h minus those in Severe-FR-48h. The grey border implies the BTH region.

The temporal variations of particulate matter from Severe-40m-48h, Severe-FR-48h and observation at six independent verification stations are shown in Figure S2~~1~~ and Figure S3~~2~~. The six independent verification stations have experienced different levels of air pollution and distributed uniformly over BTH region. It is apparently that the analysis at six stations have good agreement with observations both for $PM_{2.5}$ and PM_{10}, which can better characterize the peaks and valleys of particulate matter concentration over investigated period.

Table 3 lists the Δ RMSE, Δ CORR and AE in the simulations of particulate matter at independent stations outside the BTH region. The RMSEs and correlation coefficients have decreased and increased respectively after assimilate ground-based observations, suggesting

带格式的: 字体颜色: 红色

带格式的: 字体颜色: 红色

带格式的: 字体颜色: 红色

that the uncertainty in Severe-FR-48h has been well optimized not only in the BTH region, but also includes the whole simulation domain. The main source of these gains is generated from local initial field assimilation. Compared to the Severe-FR-48h, the analysis in Yuncheng shows that the RMSE values of $PM_{2.5}$ and PM_{10} have decreased by 98.26 and 144.56 μg m^{-3} remarkably, such a great improvement may relate to the enhanced estimation capability about state variables of particulate matter. The high values of AE also suggest that verification observation sites outside the BTH region have achieved a good Kalman gain. In previous researches, predicting heavy haze events in northern China, especially over the BTH ~~Beijing-Tianjin-Hebei~~ Region, remained a challenge when compared to other regions like Pearl River Delta and Yangtze River Delta in China (Feng et al., 2018, Gao et al., 2017). ~~The deficiency may be induced by GFS (National Centers for Environmental Prediction Global Forecast System) data, providing a poor estimation of meteorological fields in northern China, increasing the instability of atmospheric dynamics and ultimately decreasing the assimilation effect (Kong et al., 2021).~~ In this research, the analysis is propagated by meteorological elements including temperature, air pressure and wind fields come from NCEP Final analysis data, which may provide an optimal meteorological boundary conditions for the assimilation of pollutant concentration.

Table 3. Statistics about $PM_{2.5}$ and PM_{10} from analysis in the cities among neighboring provinces of BTH region. Δ RMSE (Δ CORR) represent the RMSE (correlation coefficient) from analysis minus those from Severe-FR-48h (units for Δ RMSE: μg m^{-3}).

City/	$PM_{2.5}$			PM_{10}		
Statistical variable	Δ RMSE	Δ CORR	AE	Δ RMSE	Δ CORR	AE

带格式的: 字体颜色: 红色

带格式的: 字体颜色: 红色

带格式的: 字体颜色: 红色

Taiyuan	-21.30	+0.41	23.93%	-54.8	+0.71	39.05%
Changzhi	-38.39	+0.38	65.93%	-63.06	+0.68	63.22%
Jincheng	-37.94	+0.37	66.85%	-94.32	+0.89	72.45%
Shuozhou	-27.07	+0.31	58.96%	-100.08	+0.84	69.96%
Yuncheng	-98.26	+0.67	77.85%	-144.56	+1.25	80.64%
Hohhot	-92.30	+0.67	74.53%	-121.79	+1.41	68.92%
Chifeng	-16.90	+0.55	64.95%	-38.18	+0.95	60.85%
Huludao	-38.56	+0.20	59.11%	-95.95	+1.04	65.76%
Jinzhou	-42.97	+0.21	61.17%	-46.26	+0.83	45.83%
Chaoyang	-39.37	+0.37	51.14%	-83.04	+1.23	61.86%
Jinan	-44.90	+0.63	69.71%	-71.22	+0.59	62.93%
Qingdao	-23.99	+0.27	37.98%	-72.05	+0.44	72.21%
Shouguang	-28.70	+0.21	58.03%	-48.92	+0.39	47.57%
Anyang	-35.87	+0.41	62.53%	-32.08	+0.60	33.15%
Zhengzhou	-26.26	+0.37	37.51%	-3.64	+0.42	3.73%

3.2 The sensitivity of 4D-LETKF to ensemble member size and length of assimilation window

In previous section, the research has compared the performance from assimilation experiment with 40 ensemble members and 48 hours of assimilation window length against that do not integrate hourly pollutant observations. The results fully demonstrate the ability of 4D-LETKF assimilation method to reproduce severe haze events in spatial and temporal dimensions. However, the 4D-LETKF assimilation effect is highly rely on selection of

带格式的: 字体颜色: 红色

ensemble member size and length of assimilation window, so how does the assimilation approach vary to the parameterized selection in severe haze event? It is of great meaning to conduct sensitivity experiments based on ensemble member size and length of assimilation window, compare each performance of them by statistical metrics, and summarize the general influence rule of 4D-LETKF parameter selection. Consequently, nine panels of sensitivity experiments are conducted with the selection of ensemble member size (20, 40, 60 members) and the length of assimilation window (24, 48, 72 hours) to maximize the positive innovation in this section.

Figure 8 reveals the heatmap about RMSE in each sensitivity experiment of particulate matter over verification sites among the BTH region. The results of free run experiment with different integration times (24, 48, 72 hours) are offered here for comparison with analysis which with same assimilation cycle time. The RMSEs of $PM_{2.5}$ and PM_{10} in each free run experiment exceed 60μg m^{-3} and 100μg m^{-3}, respectively. It is apparently that the 4D-LETKF performs better than the FR experiment in the simulation about $PM_{2.5}$ and PM_{10} over wide range of ensemble member sizes and assimilation window lengths, illustrating the broad applicability of 4D-LETKF data assimilation to these parameters. However, it can be found that the analysis of $PM_{2.5}$ and PM_{10} are dependent on length of assimilation window and dramatically related to ensemble member size in all sensitivity experiments. Unlike the short-lived and chemical reactive species (such as SO_2 and NO_2) which easily undergo complex and nonlinear photochemical reactions, a relative longer assimilation window length seems more suitable for assimilating ground-based particulate matter observations (Peng et al., 2017, Kong et al., 2021). A longer assimilation window length could also avoid underestimation of model spread, which

带格式的: 字体颜色: 红色

implies overconfidence in the first guess ~~avoid the underestimation of model spread and overconfidence in the first guess~~ state estimate by enough integration time of each member (Schutgens et al., 2010, Miyazaki et al., 2012a, Hunt et al., 2007). Hence, 48 or 72 hours of assimilation window length are advised to optimize the ensemble concentration trajectories. On the other hands, increasing ensemble member size efficiently reduces uncertainty in $PM_{2.5}$ and PM_{10}, as evidenced by the decrease of RMSEs from free run to assimilation experiments with 20 and 40 members. However, when compared with the results from 40 ensemble members, the accuracy of numerical simulations has not significantly improved for both $PM_{2.5}$ and PM_{10} with 60 ensemble members, indicating that 40 members are sufficient and feasible to provide a reliable estimation of the background error and analysis rather than more numerical source consumption. Considering numerical source consumption and RMSE values in the simulations of $PM_{2.5}$ and PM_{10}, the Severe-40m-48h shows more comparable to the observations when compared with the other eight panels of sensitivity experiments.

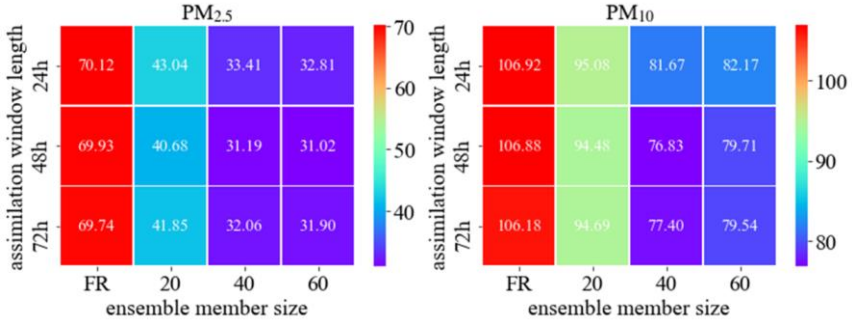

Figure 8. Heatmap about RMSE in each sensitivity experiment of particulate matter over verification sites (units: μg m^{-3}). The number in each small square represents the RMSE between observation and simulation for each combination of ensemble member size and the length of assimilation window methods.

3.3 The influence from ensemble member size to the ensemble spread

In order to explore why increasing ensemble member size can efficiently reduce the uncertainty in the analysis of $PM_{2.5}$ and PM_{10} as revealed in Figure 8, the study investigates the spatial distribution of standard deviations of $PM_{2.5}$ and $PM_{10\text{-}2.5}$ among first guess ($x^b(i)$) and analysis field ($x^a(\mathrm{i})$) in terms of ensemble members. The standard deviations of ensemble members describe how the emission perturbation propagates among the forward model, and this perturbation is driven by the underlying surface pollution emission inputs and the meteorological conditions. Therefore, the standard deviation in the first guess fields quantifies the dispersion degree of the ensemble background, substantially impacts the calculation of assimilation parameters such as ensemble state vector perturbations, and further affects the performance of particulate matter predictions.

Since the RMSE decreases with the increasing ensemble member size when 20 and 40 members are setting, and 48 hours of assimilation window length corresponds to a smaller RMSE, the study compares the spatial distribution of ensemble standard deviations from Severe-20m-48h and Severe-40m-48h to explain the relationship between ensemble member size and simulation errors in analysis result. Figure 9 depicts contour maps of the spatial distribution of temporal averaged standard deviations in the first guess and analysis of Severe-40m-48h, Severe-20m-48h and their difference for $PM_{2.5}$ and $PM_{10\text{-}2.5}$ during severe haze event. The first guess in Severe-40m-48h and Severe-20m-48h shows that the relatively high standard deviations are generally observed in southern of BTH region, while those in the northern areas are close to zero for both $PM_{2.5}$ and $PM_{10\text{-}2.5}$. High value centers are distributed in densely populated areas and urban centers including Shijiazhuang, Xingtai, Tianjin and Tangshan city,

where the standard deviations have generally exceeded 30μg m^{-3}. Combined with Figure S~~43~~, it can be seen that the areas with large concentration standard deviations correspond well with the spatial distribution of anthropogenic emission and the areas with large standard deviations of emission sources. The standard deviations of concentrations of $PM_{2.5}$ and $PM_{10-2.5}$ have closely relationship with the allocation and configuration of anthropogenic emission sources, because disturbances are only added to emission sources for each ensemble member, without disturbing the meteorological field in this haze event. The variation of difference in the third column entirely comes from increasing ensemble member size. The positive difference between Severe-40m-48h and Severe-20m-48h in first guess suggests that increasing ensemble member size leads to greater differences among each ensemble for both $PM_{2.5}$ and $PM_{10-2.5}$ over BTH areas. The high efficiency of 4D-LETKF is strongly influenced by sufficient information spread among ensemble members, which integrate spreading observational information to produce analysis from the first guess (Rubin et al., 2016). As a result, the increasing ensemble member size improves divergence for each member and facilitates the state vectors about $PM_{2.5}$ and $PM_{10-2.5}$ information spread in the first guess, which makes a better performance for Severe-40m-48h rather than Severe-20m-48h in this severe haze event. The standard deviations of $PM_{2.5}$ in analysis are generally lower than those in first guess. Due to the localization of 4D-LETKF, that is the ground-based observation data only optimized for simulation grid within a certain range, square-like areas of low standard deviations appear in the analysis of $PM_{2.5}$ both for 40 and 20 ensemble members. Nearly all assimilated stations are located at the center of low value square areas suggesting that 4D-LETKF tunes all $PM_{2.5}$ trajectories into a small range with low standard deviation at each slot of analysis by the assimilation of ground-based

带格式的: 字体颜色: 红色

observations. For $PM_{10-2.5}$, there are no square-like areas of low standard deviations in the analysis both for 40 and 20 ensemble members, indicating that the 4D-LETKF does not has an obvious limitation for $PM_{10-2.5}$ trajectories, however, the decreased standard deviations effect from the 4D-LETKF is still distinct for the particulate matter because PM_{10} consist of $PM_{2.5}$ and $PM_{10-2.5}$ in simulation. Enlarging ensemble member size is benefit to the improving of standard deviations of $PM_{2.5}$ and $PM_{10-2.5}$ in analysis, while the improving magnitude of $PM_{2.5}$ is obviously smaller than $PM_{10-2.5}$. The assimilation results are not directly influenced by the increased standard deviations in analysis. Such low increasement of standard deviations (generally below 3 μg m^{-3}) is unlikely to induce uncertainty in the fitting and averaging process, but facilitates divergence in initial conditions between forecasting members in the next assimilation cycle. In addition, Figure S54 depict the spatial distribution of standard deviation from Severe-60m-48h, Severe-20m-48h and their difference in the first guess and analysis field. It can be seen that increasing the number of ensemble member generally also improves the standard deviation in first guess and analysis over the BTH region both for $PM_{2.5}$ and $PM_{10-2.5}$. Overall, the increasement of standard deviations generated by increasing ensemble member size directly improves the information spread of ensemble members in the first guess field and the assimilation effect of 4D-LETKF, while the positive difference of standard deviation in analysis favors the variances between each initial condition in the next assimilation window during severe haze event.

带格式的: 字体颜色: 红色

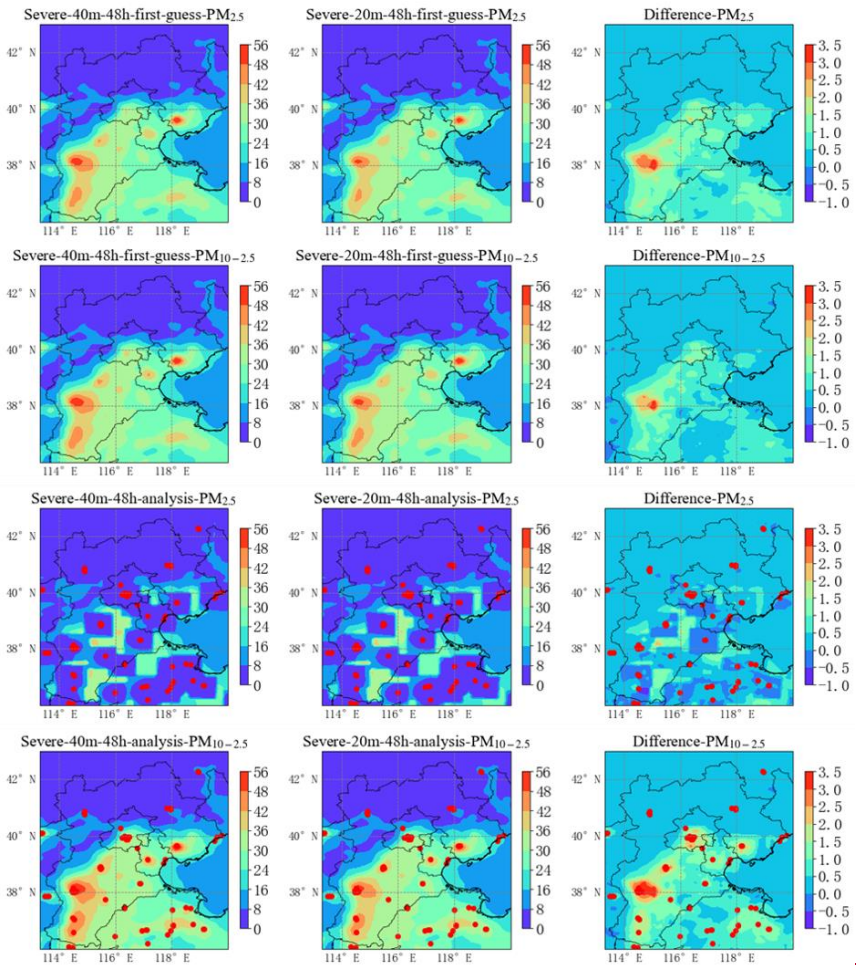
Severe-40m-48h-first-guess-PM2.5
Severe-20m-48h-first-guess-PM2.5
Difference-PM2.5
Severe-40m-48h-first-guess-PM10-2.5
Severe-20m-48h-first-guess-PM10-2.5
Difference-PM10-2.5
Severe-40m-48h-analysis-PM2.5
Severe-20m-48h-analysis-PM2.5
Difference-PM2.5
Severe-40m-48h-analysis-PM10-2.5
Severe-20m-48h-analysis-PM10-2.5
Difference-PM10-2.5
42° N
40° N
38° N
114° E
116° E
118° E
56
48
42
36
30
24
16
8
0
3.5
3.0
2.5
2.0
1.5
1.0
0.5
0.0
-0.5
-1.0

545

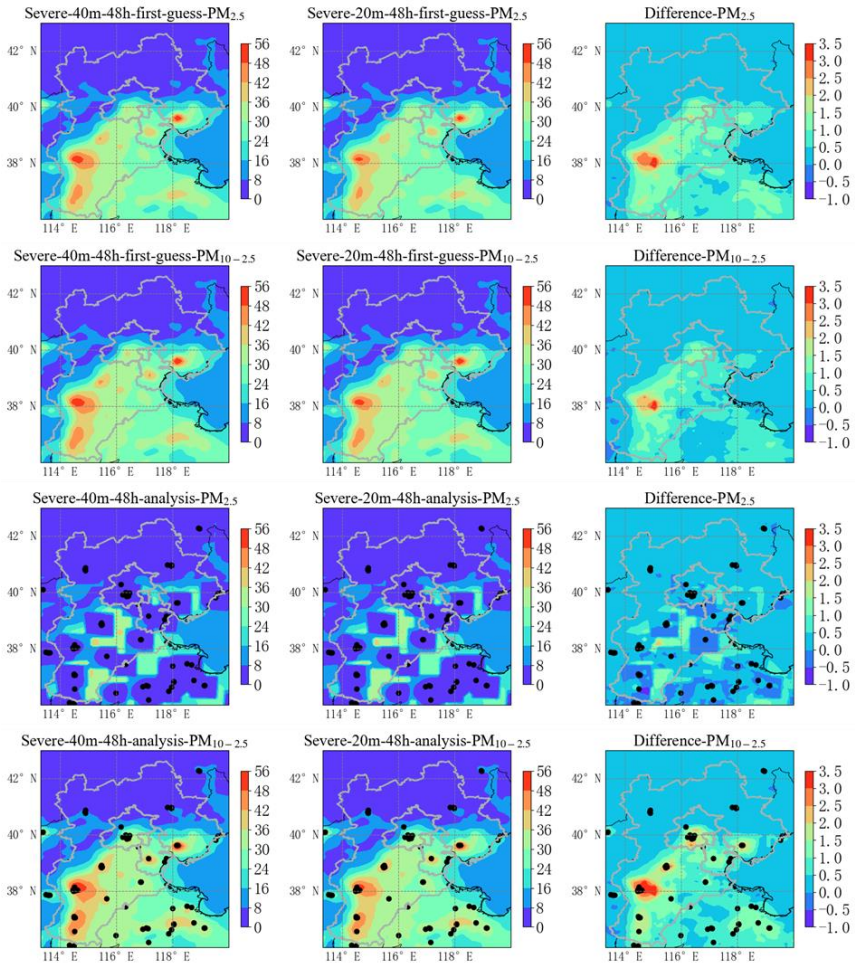

Figure 9. Contour maps of spatial distributions of temporal averaged $PM_{2.5}$ and $PM_{10\text{-}2.5}$ standard deviations in the first guess (first and second row) and analysis (third and fourth row) of Severe-40m-48h, Severe-20m-48h and their difference (Severe-40m-48h minus Severe-20m-48h) within simulation period (units: μg m^{-3}). The black ~~red~~ dots in analysis of $PM_{2.5}$ and $PM_{10\text{-}2.5}$ implies the location of assimilated stations. The grey border implies the BTH region.

带格式的: 字体颜色: 红色

带格式的: 字体颜色: 红色

In the other sides, no matter for the first guess from Severe-40m-48h or Severe-20m-48h,

the high standard deviations are found near Shijiazhuang region in Figure 9, but Shijiazhuang station (37.91N°, 114.35°E) still with larger RMSE and smaller AE in Figure 6. This seems contrary to the opinion that increasing standard deviations in the first-guess field is beneficial to raising the accuracy of pollutant simulations. Therefore, Shijiazhuang station and the stations which with high values of AE (exceed 50) and difference of standard deviation in first guess (exceed 1 μg m^{-3}) including Beijing, Tangshan, Handan, Baoding, Cangzhou, and Hengshui regions are selected to explore the temporal distribution of standard deviations difference between 40 and 20 ensemble members, so as to further advance our understanding about the relationship between ensemble member size and simulation uncertainty in 4D-LETKF system. The geographical locations of observations are shown in Figure S6 of the supplement. Figure 10 examines the temporal distribution of the standard deviation difference for $PM_{2.5}$ and $PM_{10-2.5}$ during the investigated period at Shijiazhuang station and results averaged from the selected stations. From January 17 to January 18, the standard deviation difference in first guess at Shijiazhuang station has increased drastically and exceeded up to 10 μg m^{-3} for both $PM_{2.5}$ and $PM_{10-2.5}$. This uneven temporal distribution results in a large standard deviation difference of first guess in Figure 9. This huge divergency between ensemble member may attributed to the peak pollutant levels with AQI exceeds 300 at Shijiazhuang station occurs on the January 17 as shown in Figure 3. In highly polluted environments, 40 forecasting members with different perturbations in emission sources are more likely to differ the concentration of particulate matter in first guess fields. Excessive large spread ~~high dispersion~~ of $PM_{2.5}$ and $PM_{10-2.5}$ for ensemble members may arise an over-high estimation about background error variance ~~covariances~~ and obtain a poor Kalman gain. Moreover, it can be found that the standard

带格式的: 字体颜色: 红色

带格式的: 字体颜色: 红色

带格式的: 字体颜色: 红色

带格式的: 字体颜色: 红色

deviation difference of $PM_{2.5}$ and $PM_{10-2.5}$ at Shijiazhuang station are obviously lower than the averaged from selected stations except the high dispersion time, suggesting the increasing number of ensemble members has limited impact on the spread ~~divergence~~ between each ensemble member at Shijiazhuang during these dates. Too low standard deviations imply filter divergence ~~convergence~~ near Shijiazhuang station, which may induce the underestimation of model spread, reduce the effect of observation information, and make system more certain of state estimate about particulate matter concentrations in first guess (Hunt et al., 2007). In addition, reducing uncertainty in the mixed anthropogenic emission inventory may be an important approach to avoid filter convergence near the Shijiazhuang region. Generally edited by empirical and statistical data such as anthropogenic emission factors and activity dataset, the anthropogenic emissions based on bottom-up method can hardly capture the real spatiotemporal distribution of anthropogenic emissions over China as frequently variations in energy consumption, even though the latest version. Among the southern of BTH region, the great positive innovations of particulate matter emissions in posterior estimation have been discovered in previous researches, implying that the update of underestimated emissions in this region may enlarge ensemble spread ~~enlarge the deviations between ensemble members~~ since a large quantity of emissions corresponds to a higher degree of perturbation (Peng et al., 2017, Feng et al., 2023). In a word, the perturbations added to emissions and meteorological fields needs to be executed carefully in 4D-LETKF system to avoid too high or too low ensemble spread ~~dispersion~~ degree because which determinate how analysis results weight toward observations information and first guess fields (Dai et al., 2021).

带格式的: 字体颜色: 红色

带格式的: 字体颜色: 红色

带格式的: 字体颜色: 红色

带格式的: 字体颜色: 红色

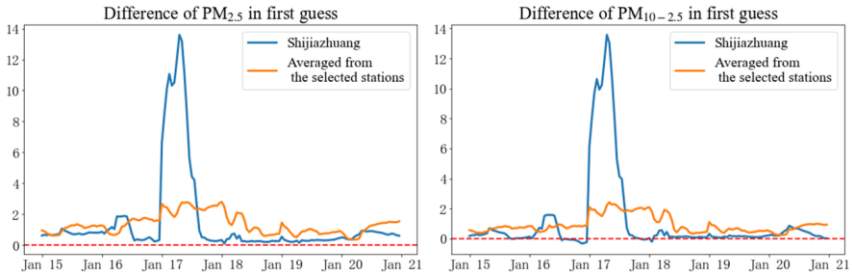

Figure 10. Temporal distribution of standard deviation difference (Severe-40m-48h minus Severe-20m-48h) in first guess for $PM_{2.5}$ and $PM_{10-2.5}$ at Shijiazhuang station and averaged from the selected stations (units: μg m^{-3}). The red dash line is zero.

The results above suggest that the increasing ensemble member size ~~,~~ enlarges ensemble spread~~strengthens divergence~~, benefits the information spread in the first guess and finally improves the simulative skill in severe haze event. However, it has not been testified whether these influence rules are also practical for a more common, and less polluted condition. Therefore, two assimilation experiments in moderate haze event, Moderate-20m-48h and Moderate-40m-48h, are performed to examine the applicable range. As shown in Figure S7~~5~~, the moderate haze event spans from 00:00 UTC 15 January 2019 to 00:00 UTC 21. This moderate event began on 15 January, with AQI increasing until 18 January, reaching a moderate level but not lasting for a long time, and then decreased on 19 and 20 January. Most areas experienced mild or moderate air pollution, with AQI generally below 200, the primary pollutant was particulate matter after calculation. The simulations of moderate haze event utilize the same anthropogenic emission inventory as used in severe haze event since two events both happen in January, thereby avoids the additional influence introduce from emission source variation and the perturbations to information spread and assimilation effect.

Figure S8~~6~~ shows the simulated concentrations of $PM_{2.5}$ and PM_{10} against ground-based

带格式的: 字体颜色: 红色

observations during moderate air pollution event. The RMSEs of $PM_{2.5}$ in Moderate-FR-48h, Moderate-20m-48h and Moderate-40m-48h are 40.40, 24.12 and 18.52μg m^{-3}, respectively, and the RMSEs of PM_{10} are 73.47, 67.81 and 57.04 μg m^{-3} respectively. The concentrations of $PM_{2.5}$ and PM_{10} in assimilation experiments are more in agreement with observations, suggesting the validation of 4D-LETKF initial condition adjustment in moderate haze event. The phenomena that the simulation error of $PM_{2.5}$ and PM_{10} decrease with increasing ensemble member size are same with those characteristics have shown in severe haze event before.

Similar to Figure 9, Figure S9~~7~~ presents the spatial distributions of standard deviations about $PM_{2.5}$ and PM_{10} in the first guess of Moderate-40m-48h, Moderate-20m-48h and their difference. The relatively smaller magnitude of standard deviation difference in first guess may relate to relatively low $PM_{2.5}$ and PM_{10} concentrations in moderate haze event. Positive difference in first guess and analysis for particulate matter implies the Moderate-40m-48h obtains a higher diversity of ensemble members than Moderate-20m-48h, and which are also similar with those happen in the severe haze event.

4. Summary

The numerical reproduction ~~simulation~~ of severe haze events with AQI ~~air quality index~~ larger than 200 has been a challenging problem in the field of atmospheric pollution for a long time. In this research, a WRF-Chem/4D-LETKF coupled data assimilation system has been successfully developed by ensemble member with perturbed anthropogenic emissions to improve the simulative skill of particulate matter in severe haze event during the winter of 2020. The research validated the effectiveness of 4D-LETKF data assimilation, discussed the optimal parameter combination of ensemble member size and length of assimilation window for 4D-

带格式的: 字体颜色: 红色

带格式的: 字体: (默认) Times New Roman, (中文) 宋体, 11 磅, 字体颜色: 红色

带格式的: 字体颜色: 红色

带格式的: 字体颜色: 红色

LETKF assimilation system, summarized and explained the influence rules from parametric selection to the 4D-LETKF assimilation effect during severe and moderate haze event.

It is concluded that the Severe-40m-48h experiment shows the best performance in the simulations of $PM_{2.5}$ and PM_{10} after comparing the statistical errors and computing resource consumption across multiple sensitivity analyses, with the RMSEs of 31.19 and 76.83μg m^{-3} for $PM_{2.5}$ and PM_{10} in severe haze event. Severe-40m-48h optimizes the underestimation of particulate matter concentrations in Severe-FR-48h, and remarkably improves the simulation accuracy in the entire BTH region and neighboring provinces. For example, the RMSEs of $PM_{2.5}$ in Baoding, Hengshui and Cangzhou decrease to 29.85, 18.98 and 19.06 μg m^{-3} respectively, from 80.55, 55.22 and 76.32 μg m^{-3} in Severe-FR-48h. Severe-40m-48h is also capable of retrieving the peaks and valleys of particulate matter concentration over the investigated period. To examine the dependence of the assimilation effect of 4D-LETKF, nine panels of sensitivity tests were conducted according to ensemble member size and length of assimilation window. The findings suggest that the simulation accuracy of $PM_{2.5}$ and PM_{10} can be strongly improved by the increasing ensemble member size from 20 to 40. A relative longer assimilation window length such as 48 or 72 hours combine with 40 ensemble member size is advised in 4D-LETKF assimilation system. In view of performance of ensemble member, increasing ensemble member size improves ~~divergence~~ ensemble spread among each forecasting member, facilitates the spread of state vectors about $PM_{2.5}$ and PM_{10} information in the first guess, favors the variances between each initial condition in the next assimilation window and leads to better performance in simulation of severe haze event. A similar conclusion can also be draw from the moderate haze event, suggesting that this influence rule

带格式的: 字体颜色: 红色

带格式的: 字体颜色: 红色

is applicable in both severe and moderate haze conditions.

There are still some deficiencies in this research. Although we have performed data quality control in this study, we did not use approaches such as super-observations to improving the correspondence between grid points and observations (Jin et al., 2022, Miyazaki et al., 2012a), which may increase the representational error and result in the possibility of two stations with different concentrations interpolating in the same grid. Improving the spatial resolution of forward model or introducing super observations may mitigate this problem (Miyazaki et al., 2012b, Feng et al., 2020b). Furthermore, the concentration of state variables about particulate matters in initial conditions are optimized in this study, but there still remain large uncertainties in anthropogenic emission data, which is an important chemical boundary input for pollutant simulations. These uncertainties sources may play a significant role in the over- or underestimation of pollutant ensemble modeling. The anthropogenic emissions inversion based on Ensemble Kalman filter and their variants is recognized as an effective approach for reducing uncertainty in anthropogenic emission sources (Peng et al., 2018, Feng et al., 2020a, Chen et al., 2019b). The jointly adjust initial conditions and emissions source with 4D-LETKF is the focus of future work to further improving the forecast skills about air pollutants during heavy pollution events.

CRediT authorship contribution statement

Jianyu Lin: Conceptualization, Formal analysis, Visualization. **Tie Dai**: Investigation, Methodology, Resources, Supervision. **LiFang Sheng**: Funding acquisition, Project administration. **Weihang Zhang**: Writing - original draft, Data curation. **Shangfei Hai**: Writing

682 - review and editing. **Yawen Kong**: Validation.

683

684 Declaration of competing interest

685 The authors declare that they have no conflict of interest.

686 Acknowledgements

687

688 Financial support. This work is supported by the National Natural Science Foundation of China

689 (No. 42275191), National Natural Science Funds of China (42375190).

690

691 Code and data availability

692 The code and data in this research are available in https://zenodo.org/records/14010521, and

693 we are grateful to the relevant researchers who make contributions to WRF-Chem model and

694 LETKF method (Miyoshi, 2024).

695

696 Reference

697

698 Anderson, J. L.: An adaptive covariance inflation error correction algorithm for ensemble filters,

699 Tellus, 59A, 210–224, https://doi.org/10.1111/j.1600-0870.2006.00216.x, 2007.

700

701 Bao, J., Yang, X., Zhao, Z., Wang, Z., Yu, C., Li, X.: The spatial-temporal characteristics of air

702 pollution in China from 2001-2014, Int. J. Environ. Res. Publ.Health, 12 (12), 15875e15887,

703 https://doi.org/10.3390/ijerph121215029, 2015.

带格式的: 字体颜色: 红色

带格式的: 字体颜色: 红色

带格式的: 字体颜色: 红色

Barbu, A. L., Segers, A. J., Schaap, M., Heemink, A. W., and Builtjes, P. J. H.: A multi-component data assimilation experiment directed to sulphur dioxide and sulphate over Europe, Atmospheric Environment, 43(9), 1622–1631, https://doi.org/10.1016/j.atmosenv.2008.12.005, 2009.

Benedetti, A., Morcrette, J., Boucher, O., Dethof, A., Engelen, R. J., Fisher, M., Flentje, H., Huneeus, N., Jones, L., Kaiser, J. W., Kinne, S., Mangold, A., Razinger, M., Simmons, A. J., and Suttie, M.: Aerosol analysis and forecast in the European Centre for Medium-Range Weather Forecasts Integrated Forecast System: 2. Data assimilation, J. Geophys. Res., 114, D13205, https://doi.org/10.1029/2008JD011115, 2009.

Cheng, Y., Dai, T., Goto, D., Schutgens, N. A. J., Shi, G., and Nakajima, T.: Investigating the assimilation of CALIPSO global aerosol vertical observations using a four-dimensional ensemble Kalman filter, Atmos. Chem. Phys, 19, 13445–13467, https://doi.org/10.5194/acp-19-13445-2019, 2019.

Chen, D., Liu, Z., Ban, J., and Chen, M.: The 2015 and 2016 wintertime air pollution in China: SO_2 emission changes derived from a WRF-Chem/EnKF coupled data assimilation system, Atmos. Chem. Phys, 19, 8619–8650, https://doi.org/10.5194/acp-19-8619-2019, 2019a.

Chen, D., Liu, Z., Ban, J., Zhao, P., and Chen, M.: Retrospective analysis of 2015–2017

wintertime $PM_{2.5}$ in China: response to emission regulations and the role of meteorology, Atmos. Chem. Phys., 19, 7409–7427, https://doi.org/10.5194/acp-19-7409-2019, 2019b.

Dai, T., Cheng, Y., Goto, D., Li, Y., Tang, X., Shi, G., and Nakajima, T.: Revealing the sulfur dioxide emission reductions in China by assimilating surface observations in WRF-Chem, Atmos. Chem. Phys., 21, 4357–4379, https://doi.org/10.5194/acp-21-4357-2021, 2021.

Dai, T., Cheng, Y., Suzuki, K., Goto, D., Kikuchi, M., Schutgens, N. A. J., Yoshida, M., Zhang, P., Husi, L., Shi, G., and Nakajima, T.: Hourly Aerosol Assimilation of Himawari-8 AOT Using the Four-Dimensional Local Ensemble Transform Kalman Filter, J. Adv. Model. Earth Syst., 11, 680–711, https://doi.org/10.1029/2018MS001475, 2019.

Elbern, H., Strunk, A., Schmidt, H., and Talagrand, O.: Emission rate and chemical state estimation by 4-dimensional variational inversion, Atmospheric Chemistry and Physics, 7(14), 3749–3769, https://doi.org/10.5194/acp-7-3749-2007, 2007.

Evensen, G.: Sequential data assimilation with a nonlinear quasi-geostrophic model using Monte Carlo methods to forecast error statistics, Journal of Geophysical Research: Oceans, 99, 10143–10162, https://doi.org/10.1029/94JC00572, 1994.

Evensen, G.: The Ensemble Kalman Filter: theoretical formulation and practical implementation, Ocean Dynam, 53, 343–367, https://doi.org/10.1007/s10236-003-0036-9,

2003.

Feng, S., Jiang, F., Jiang, Z., Wang, H., Cai, Z., and Zhang, L.: Impact of 3DVAR assimilation of surface $PM_{2.5}$ observations on $PM_{2.5}$ forecasts over China during wintertime, Atmospheric Environment, 187, 34-49, https://doi.org/10.1016/j.atmosenv.2018.05.049, 2018.

Feng, S., Jiang, F., Wang, H., Wang, H., Ju, W., Shen, Y., Zheng, Y., Wu, Z., and Ding, A.: NOx emission changes over China during the COVID-19 epidemic inferred from surface NO_2 observations, Geophysical Research Letters, 47, e2020GL090080, https://doi.org/10.1029/2020GL090080, 2020a.

Feng, S., Jiang, F., Wu, Z., Wang, H., Ju, W., and Wang, H.: CO emissions inferred from surface CO observations over China in December 2013 and 2017, Journal of Geophysical Research: Atmospheres, 125, https://doi.org/10.1029/2019JD031808, 2020b.

Feng, S., Jiang, F., Wu, Z., Wang, H., He, W., Shen, Y., Zhang, L., Zheng, Y., Lou, C., Jiang, Z., and Ju, W.: A Regional multi-Air Pollutant Assimilation System (RAPAS v1.0) for emission estimates: system development and application, Geosci. Model Dev., 16, 5949–5977, https://doi.org/10.5194/gmd-16-5949-2023, 2023.

Gao, M., Saide, P. E., Xin, J., Wang, Y., Liu, Z., Wang, Y., Wang, Z., Pagowski, M., Guttikunda, S. K., and Carmichael, G. R.: Estimates of Health Impacts and Radiative Forcing in Winter

Haze in Eastern China through Constraints of Surface $PM_{2.5}$ Predictions, Environmental Science & Technology, 51(4), 2178-2185, https://doi.org/10.1021/acs.est.6b03745, 2017.

Grell, G. A.: Prognostic Evaluation of Assumptions Used by Cumulus Parameterizations, Mon. Wea. Rev., 121, 764–787, https://doi.org/10.1175/1520-0493(1993)121<0764:PEOAUB>2.0.CO;2, 1993.

Grell, G., Peckham, S. E., Schmitz, R., McKeen, S. A., Frost, G., Skamarock, W. C., and Eder, B.: Fully coupled "online" chemistry within the WRF model, Atmos. Environ, 39, 6957–6975, https://doi.org/10.1016/j.atmosenv.2005.04.027, 2005.

Guenther, A., Hewitt, C. N., Erickson, D., Fall, R., Geron, C., Graedel, T., Harley, P., Klinger, L., Lerdau, M., Mckay, W. A., Pierce, T., Scholes, B., Steinbrecher, R., Tallamraju, R., Taylor, J., and Zimmerman, P.: A global model of natural volatile organic compound emissions, Journal of Geophysical Research: Atmospheres, 100, 8873–8892, https://doi.org/10.1029/94JD02950, 1995.

Hong, S., Noh, Y., and Dudhia, J.: A new vertical diffusion package with an explicit treatment of entrainment processes, Mon. Wea. Rev, 134, 2318–2341, https://doi.org/10.1175/MWR3199.1, 2006.

Huang, X.Y., Xiao, Q., Barker, D. M., Zhang, X., Michalakes, J., Huang, W., Henderson, T., Bray, J., Chen, Y., Ma, Z., Dudhia, J., Guo, Y., Zhang, X., Won, D., Lin, H., and Kuo, Y.: Four-

792 dimensional variational data assimilation for WRF: Formulation and preliminary results, Mon.
793 Weather Rev, 137, 299–314, https://doi.org/10.1175/2008MWR2577.1, 2009.
794
795 Hunt, B. R., Kalnay, E., Kostelich, E. J., Ott, E., Patil, D. J., Sauer, T., Szunyogh, I., Yorke, J.
796 A., and Zimin, A. V.: Four-dimensional ensemble Kalman filtering, Tellus A: Dynamic
797 Meteorology and Oceanography, 56(4), 273–277, https://doi.org/10.3402/tellusa.v56i4.14424,
798 2004.
799
800 Hunt, B. R., Kostelich, E. J., and Szunyogh, I.: Efficient data assimilation for spatiotemporal
801 chaos: a local ensemble transform Kalman filter, Physica D: Nonlinear Phenomena, 230, 112–
802 126, https://doi.org/10.1016/j.physd.2006.11.008, 2007.
803
804 Iacono, M. J., Delamere, J. S., Mlawer, E. J., Shephard, M. W., Clough, S. A., and Collins, W.
805 D.: Radiative forcing by long–lived greenhouse gases: Calculations with the AER radiative
806 transfer models, J. Geophys. Res., 113, D13103, https://doi.org/10.1029/2008JD009944, 2008.
807
808 Jin, J., Pang, M., Segers, A., Han, W., Fang, L., Li, B., Feng, H., Lin, H. X., and Liao, H.:
809 Inverse modeling of the 2021 spring super dust storms in East Asia, Atmos, Chem. Phys., 22,
810 6393–6410, https://doi.org/10.5194/acp-22-6393-2022, 2022.
811
812 Kong, L., Tang, X., Zhu, J., Wang, Z., Sun, Y., Fu, P., Gao, M., Wu, H., Lu, M., Wu, Q., Huang,
813 S., Sui, W., Li, J., Pan, X., Wu, L., Akimoto, H., and Carmichael, G. R.: Unbalanced emission
814 reductions of different species and sectors in China during COVID-19 lockdown derived by

multi-species surface observation assimilation, Atmos. Chem. Phys., 23, 6217–6240, https://doi.org/10.5194/acp-23-6217-2023, 2023.

Kong, Y., Sheng, L., Li, Y., Zhang, W., Zhou, Y., Wang, W., and Zhao, Y.: Improving $PM_{2.5}$ forecast during haze episodes over China based on a coupled 4D-LETKF and WRF-Chem system, Atmospheric Research, 249, 105366, https://doi.org/10.1016/j.atmosres.2020.105366, 2021.

Lorenc, A.C.: Analysis methods for numerical weather prediction, Q. J. R. Meteorol. Soc., 112, 1177–1194, https://doi.org/10.1002/qj.49711247414, 1986.

Luo, X., Tang, X., Wang, H., Kong, L., Wu, H., Wang, W., SONG, Y., Luo, H., Wang, Y., Zhu, J., and Wang, Z.: Investigating the Changes in Air Pollutant Emissions over the Beijing-Tianjin-Hebei Region in February from 2014 to 2019 through an Inverse Emission Method, Adv. Atmos. Sci. 40, 601–618, https://doi.org/10.1007/s00376-022-2039-9, 2023.

Ma, C., Wang, T., Jiang, Z., Wu, H., Zhao, M., Zhuang, B., Li, S., Xie, M., Li, M., Liu, J., and Wu, R.: Importance of bias correction in data assimilation of multiple observations over eastern China using WRF-Chem/DART, Journal of Geophysical Research: Atmospheres, 125, e2019JD031465, https://doi.org/10.1029/2019JD031465, 2020.

Miyoshi, T., Yamane, S., and Enomoto, T.: Localizing the Error Covariance by Physical

837 Distances within a Local Ensemble Transform Kalman Filter (LETKF), Scient. Online Lett.
838 Atmos., 3, 89–92, https://doi.org/10.2151/sola.2007-023, 2007.
839
840 Morrison, H., Thompson, G., and Tatarskii, V.: Impact of Cloud Microphysics on the
841 Development of Trailing Stratiform Precipitation in a Simulated Squall Line: Comparison of
842 One– and Two–Moment Schemes, Mon. Wea. Rev., **137**, 991–1007,
843 https://doi.org/10.1175/2008MWR2556.1, 2009.
844
845 Miyazaki, K., Eskes, H. J., and Sudo, K.: Global NOx emission estimates derived from an
846 assimilation of OMI tropospheric NO_2 columns, Atmos. Chem. Phys., 12, 2263–2288,
847 https://doi.org/10.5194/acp-12-2263-2012, 2012a.
848
849 Miyazaki, K., Eskes, H. J., Sudo, K., Takigawa, M., Weele, M. van., and Boersma, K. E.:
850 Simultaneous assimilation of satellite NO_2, O_3, CO, and HNO_3 data for the analysis of
851 tropospheric chemical composition and emissions, Atmos. Chem. Phys., 12, 9545–9579,
852 https://doi.org/10.5194/acp-12-9545-2012, 2012b.
853
854 Miyoshi, T.: LETKF source codes, GitHub, available at: https://github.com/takemasa-
855 miyoshi/letkf, last access: 1 January 2024.
856
857 Ott, E., Hunt, B. R., Szunyogh, I., Zimin, A. V., Kostelich, E. J., Corazza, M., Kalnay, E., Patil,
858 D. J., and Yorke, J. A.: A local ensemble Kalman filter for atmospheric data assimilation. Tellus
859 A, 56, 415–428, https://doi.org/10.1111/j.1600-0870.2004.00076.x, 2004.
860

Pagowski, M., and Grell, G. A.: Experiments with the assimilation of fine aerosols using an ensemble Kalman filter, Journal of Geophysical Research, 117, D21302, https://doi.org/10.1029/2012JD018333, 2012.

Parrish, D. F. and Derber, J. C.: The National Meteorological Center's Spectral Statistical-Interpolation Analysis System, Mon. Weather Rev., 120, 1747–1763, https://doi.org/10.1175/1520-0493(1992)120<1747:TNMCSS>2.0.CO;2, 1992.

Peng, Z., Liu, Z., Chen, D., and Ban, J.: Improving $PM_{2.5}$ forecast over China by the joint adjustment of initial conditions and source emissions with an ensemble Kalman filter, Atmos. Chem. Phys., 17, 4837–4855, https://doi.org/10.5194/acp-17-4837-2017, 2017.

Peng, Z., Lei, L., Liu, Z., Sun, J., Ding, A., Ban, J., Chen, D., Kou, X., and Chu, K.: The impact of multi-species surface chemical observation assimilation on air quality forecasts in China, Atmos. Chem. Phys., 18, 17387–17404, https://doi.org/10.5194/acp-18-17387-2018, 2018.

Rubin, J. I., Reid, J. S., Hansen, J. A., Anderson, J. L., Collins, N., Hoar, T. J., Hogan, T., Lynch, P., McLay, J., Reynolds, C. A., Sessions, W. R., Westphal, D. L., and Zhang, J.: Development of the Ensemble Navy Aerosol Analysis Prediction System (ENAAPS) and its application of the Data Assimilation Research Testbed (DART) in support of aerosol forecasting, Atmos. Chem. Phys., 16, 3927–3951, https://doi.org/10.5194/acp-16-3927-2016, 2016.

Schutgens, N. A. J., Miyoshi, T., Takemura, T., and Nakajima, T.: Sensitivity tests for an ensemble Kalman filter for aerosol assimilation, Atmos. Chem. Phys., 10, 6583–6600, https://doi.org/10.5194/acp-10-6583-2010, 2010.

Sun, W., Liu, Z., Chen, D., Zhao, P., and Chen, M.: Development and application of the WRFDA-Chem three-dimensional variational (3DVAR) system: aiming to improve air quality forecasting and diagnose model deficiencies, Atmos. Chem. Phys., 20, 9311–9329, https://doi.org/10.5194/acp-20-9311-2020, 2020.

Schwartz, C. S., Liu, Z., Lin, H. C., and McKeen, S. A.: Simultaneous three-dimensional variational assimilation of surface fine particulate matter and MODIS aerosol optical depth, J. Geophys. Res., 117, D13202, https://doi.org/10.1029/2011JD017383, 2012.

Stockwell, W. R., Kirchner, F., Kuhn, M., and Seefeld, S.: A new mechanism for regional atmospheric chemistry modeling, J. Geophys. Res., 102, 25847–25879, https://doi.org/10.1029/97JD00849, 1997.

Tewari, M., Chen, F., Wang, W., Dudhia, J., LeMone, M. A., Mitchell, K., Ek, M., Gayno, G., Wegiel, J., and Cuenca, R. H.: Implementation and verification of the unified NOAH land surface model in the WRF model, 20th conference on weather analysis and forecasting/16th conference on numerical weather prediction, pp. 11–15, 2004.

van Donkelaar, A., Martin, R.V., Brauer, M., Hsu, N. C., Kahn, R. A., Levy, R. C., Lyapustin, A., Sayer, A. M., and Winker, D. M.: Global estimates of fine particulate matter using a combined geophysical-statistical method with information from satellites, models, and monitors, Environ. Sci. Technol, 50, 3762–3772, https://doi.org/10.1021/acs.est.5b05833, 2016.

Wang, Z., Li, J., Wang, Z., Yang, W., Tang, X., Ge, B., Yan, P., Zhu, L., Chen, X., and Chen, H.: Modeling study of regional severe hazes over mid-eastern China in January 2013 and its implications on pollution prevention and control, Sci. China-Earth Sci., 57, 3–13, https://doi.org/10.1007/s11430-013-4793-0, 2014.

Whitaker, J. S. and Hamill, T. M.: Ensemble data assimilation without perturbed observations, Mon. Weather Rev., 130, 1913–1924, https://doi.org/10.1175/1520-0493(2002)130<1913:EDAWPO>2.0.CO;2, 2002.

Yan, S., Cao, H., Chen, Y., Wu, C., and Fan, H.: Spatial and temporal characteristics of air quality and air pollutants in 2013 in Beijing, Environ Sci Pollut Res., 23, 13996–14007, https://doi.org/10.1007/s11356-016-6518-3, 2016.

Yumimoto, K., and Takemura, T.: Direct radiative effect of aerosols estimated using ensemble-based data assimilation in a global aerosol climate model, Geophysical Research Letters, 38, L21802, https://doi.org/10.1029/2011GL049258, 2011.

927 Zheng, B., Cheng, J., Geng, G., Wang, X., Li, M., Shi, Q., Qi, J., Lei, Y., Zhang, Q., He, K.:
928 Mapping anthropogenic emissions in China at 1 km spatial resolution and its application in air
929 quality modeling, Science Bulletin, 66(6), 612-620, https://doi.org/10.1016/j.scib.2020.12.008,
930 2021.
931
932 Zhang, L., Li, Q., Wang, T., Ahmadov, R., Zhang, Q., Li, M., and Lv, M.: Combined impacts
933 of nitrous acid and nitryl chloride on lower-tropospheric ozone: new module development in
934 WRF-Chem and application to China, Atmos. Chem. Phys., 17, 9733–9750,
935 https://doi.org/10.5194/acp-17-9733-2017, 2017.
936
937 Zhang, Q., Streets, D. G., Carmichael, G. R., He, K. B., Huo, H., Kannari, A., Klimont, Z., Park,
938 I. S., Reddy, S., Fu, J. S., Chen, D., Duan, L., Lei, Y., Wang, L. T., and Yao, Z. L.: Asian
939 emissions in 2006 for the NASA INTEX-B mission, Atmos. Chem. Phys., 9, 5131–5153,
940 https://doi.org/10.5194/acp-9-5131-2009, 2009.
941
942 Zhao, Y., Greybush, S. J., Wilson, R. J., Hoffman, R. N., and Kalnay, E.: Impact of assimilation
943 window length on diurnal features in a Mars atmospheric analysis, Tellus A, 67, 26042,
944 https://doi.org/10.3402/tellusa.v67.26042, 2015.
945
946 Zhang, Q., Ma, Q., Zhao, B., Liu, X., Wang, Y., Jia, B., and Zhang, X.: Winter haze over North
947 China Plain from 2009 to 2016: Influence of emission and meteorology, Environmental
948 Pollution, 242(B), 1308-1318, https://doi.org/10.1016/j.envpol.2018.08.019, 2018.

Zhan, D., Kwan, M., Zhang, W., Yu, X., Meng, B., and Liu, Q : The driving factors of air quality index in China, Journal of Cleaner Production, 197, 1, 1342-1351, https://doi.org/10.1016/j.jclepro.2018.06.108, 2018.

带格式的: 字体颜色: 红色

带格式的: 字体颜色: 红色

带格式的: 字体颜色: 红色

Supplement of

Sensitivity Studies of Four-Dimensional Local Ensemble Transform Kalman Filter Coupled With WRF-Chem Version 3.9.1 for Improving Particulate Matter Simulation Accuracy

The formulation of RMSE, and correlation coefficient are shown below:

$$RMSE = \sqrt{\frac{1}{N}\sum_{i=1}^{N}(M_i - O_i)^2}$$

$$CORR = \frac{\sum_{i=1}^{N}(O_i - \bar{O})(M_i - \bar{M})}{\sqrt{\sum_{i=1}^{N}(O_i - \bar{O})^2 \sum_{i=1}^{N}(M_i - \bar{M})^2}}$$

N is the total number of observations. I and J is the sample number of simulation and observation. M is the simulation results and the O is observation.

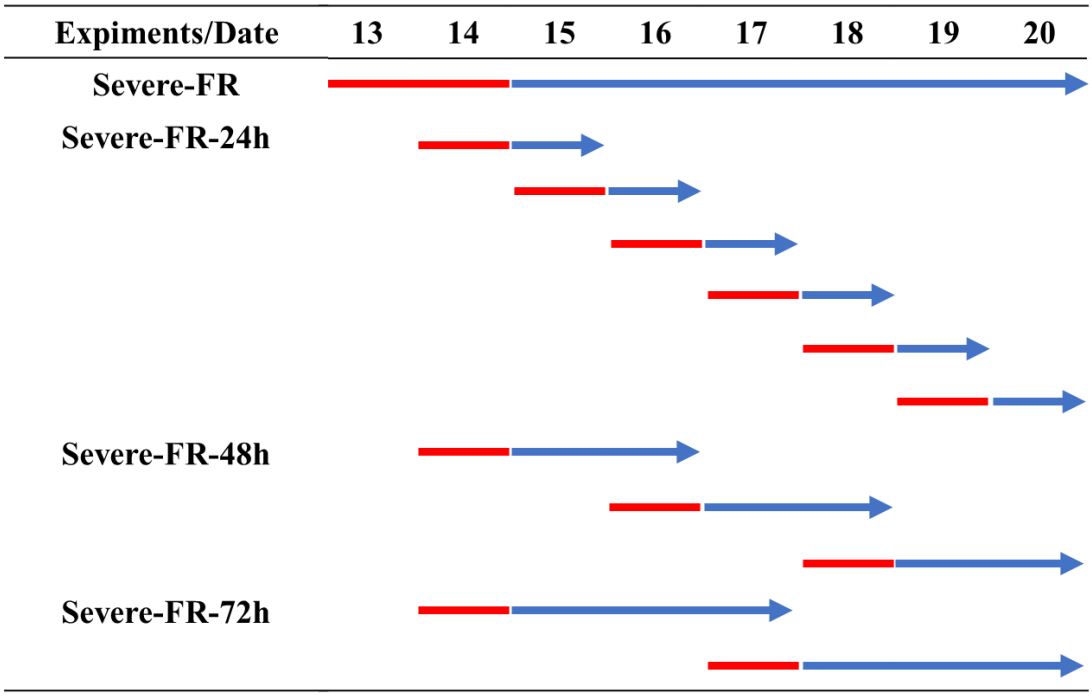

Figure S1. The spin up time (red bar) and integration time (blue arrows) of control

experiments in this research.

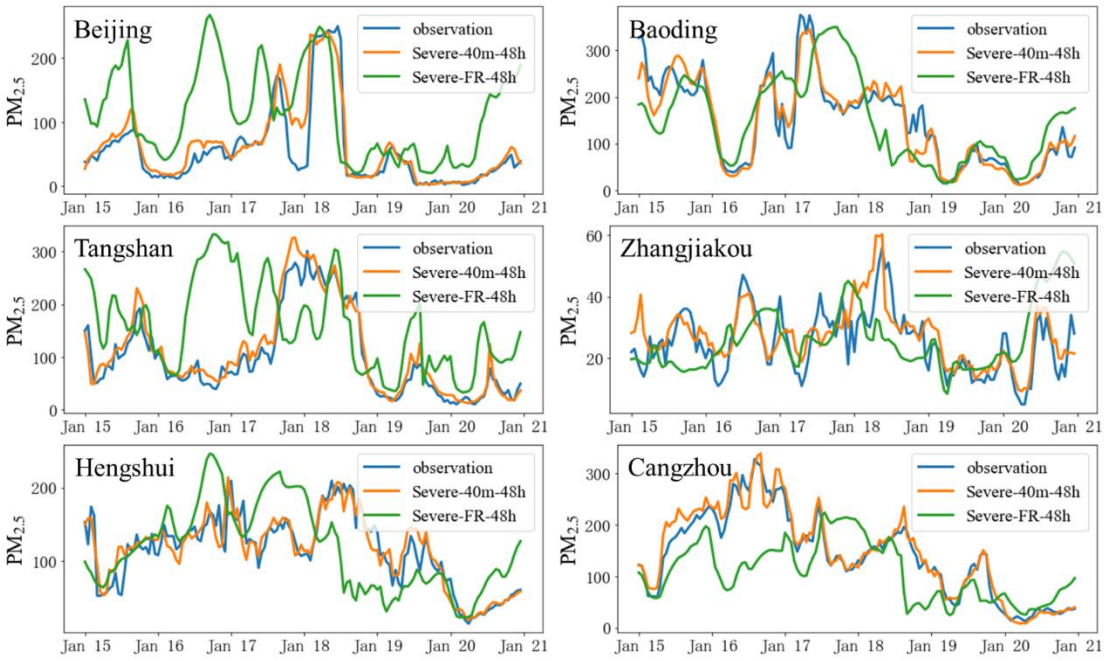

Figure S2. Temporal variations of $PM_{2.5}$ from Severe-40m-48h, Severe-FR-48h and observation at six independent verification stations (units: μg m^{-3}).

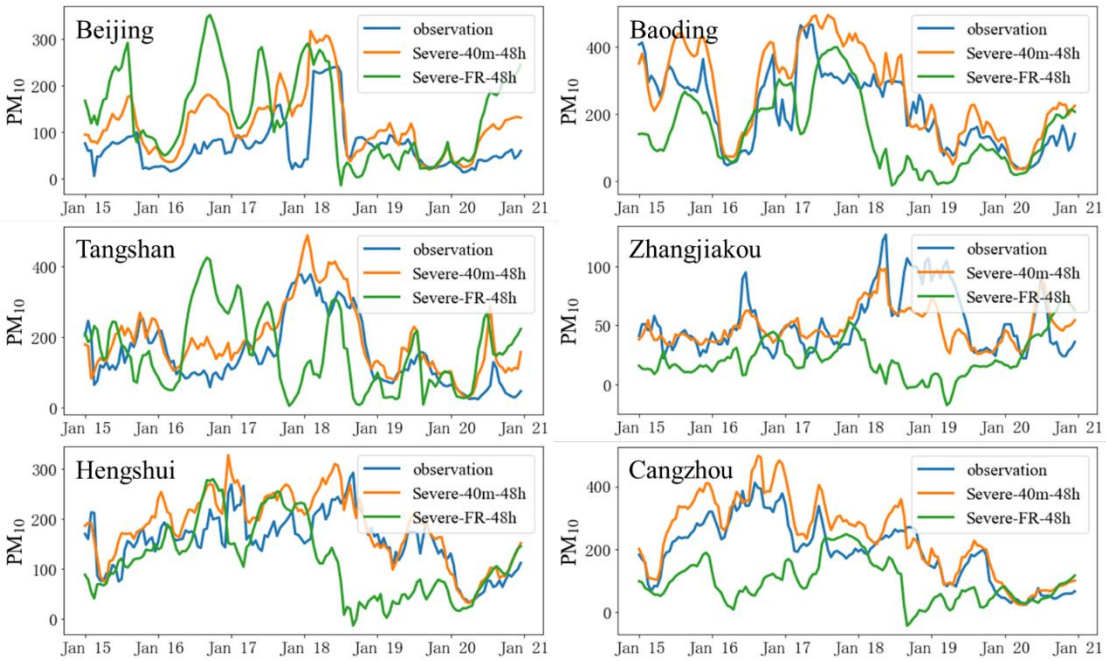

Figure S3. Similar with Figure S2 but for PM_{10}.

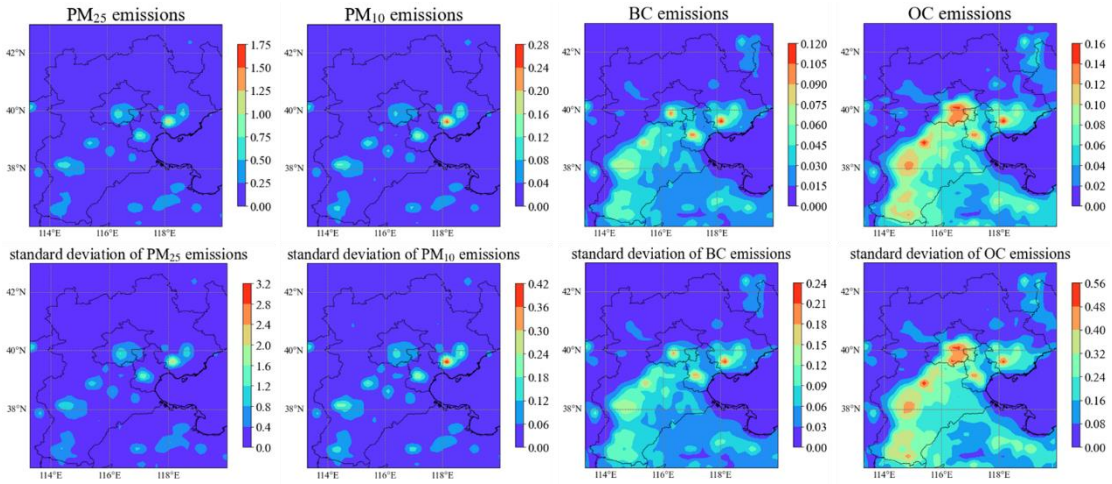

Figure S4. Contour maps about spatial distribution of anthropogenic $PM_{2.5}$, PM_{10}, BC and OC emissions in first row (units: $\mu g\ m^{-2}\ s^{-1}$) and their standard deviations calculated from 40 ensemble members in second row.

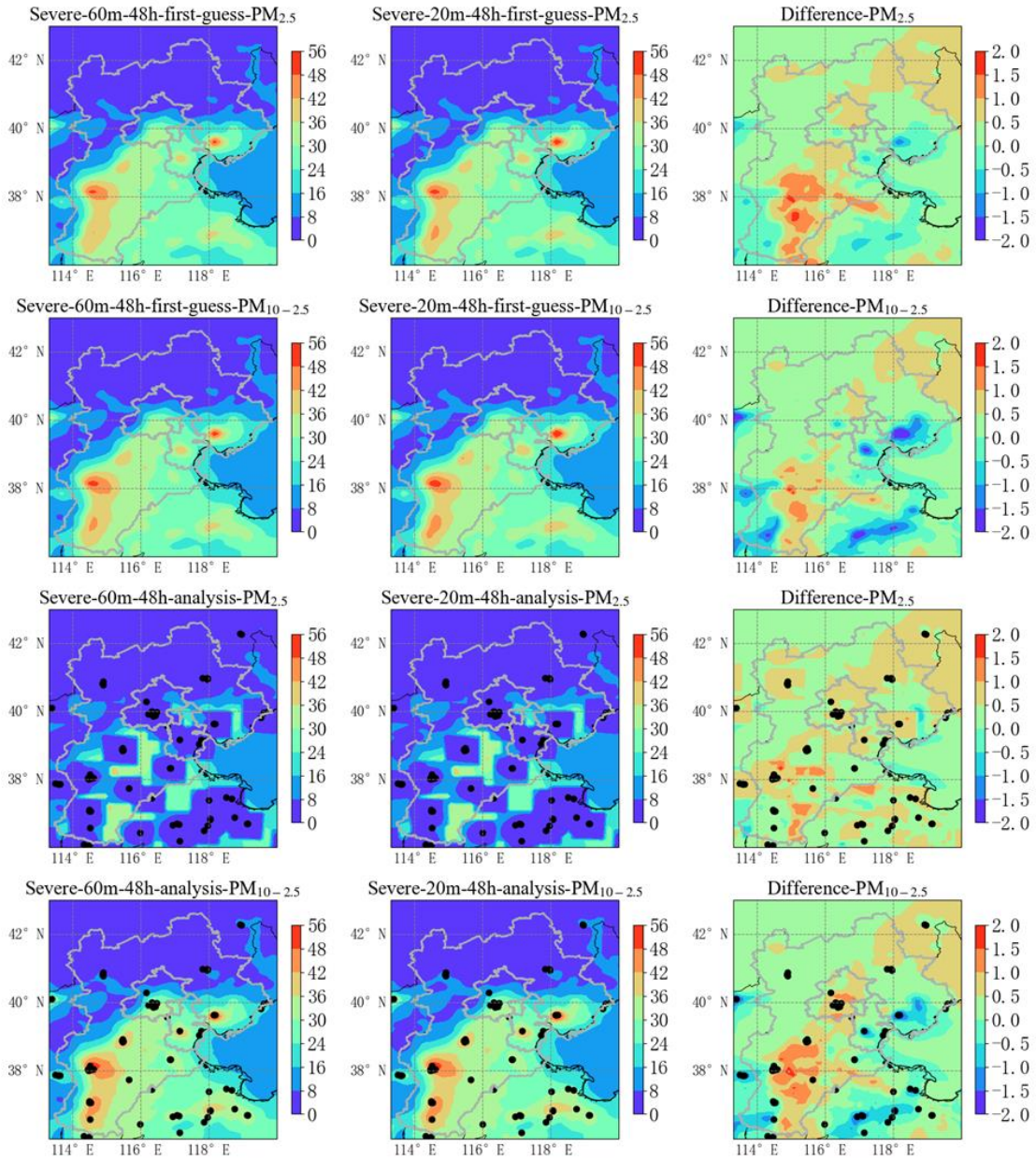

Figure S5. Contour maps of spatial distributions of temporal averaged $PM_{2.5}$ and $PM_{10-2.5}$ standard deviations in the first guess (first and second row) and analysis (third and fourth row) of (Severe-60m-48h minus Severe-20m-48h) within simulation period (units: μg m^{-3}). The black dots in analysis of $PM_{2.5}$ and $PM_{10-2.5}$ implies the location of assimilated stations. The grey border implies the BTH region.

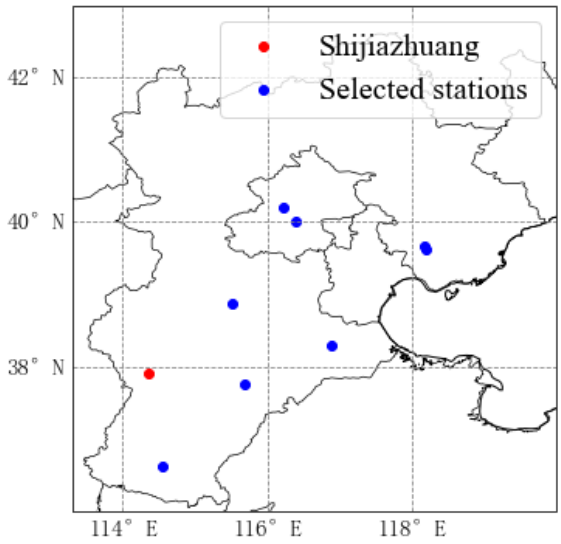

Figure S6. The geographical locations of observations of Shijiazhuang and selected stations.

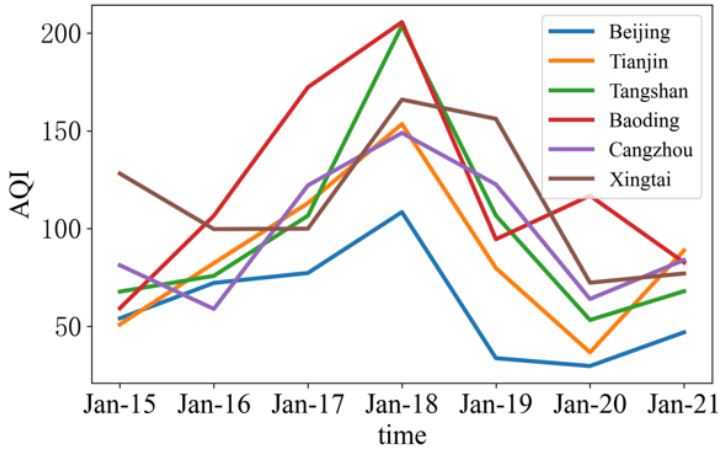

Figure S7. Temporal variation about air quality index at six representative sites in moderate haze event.

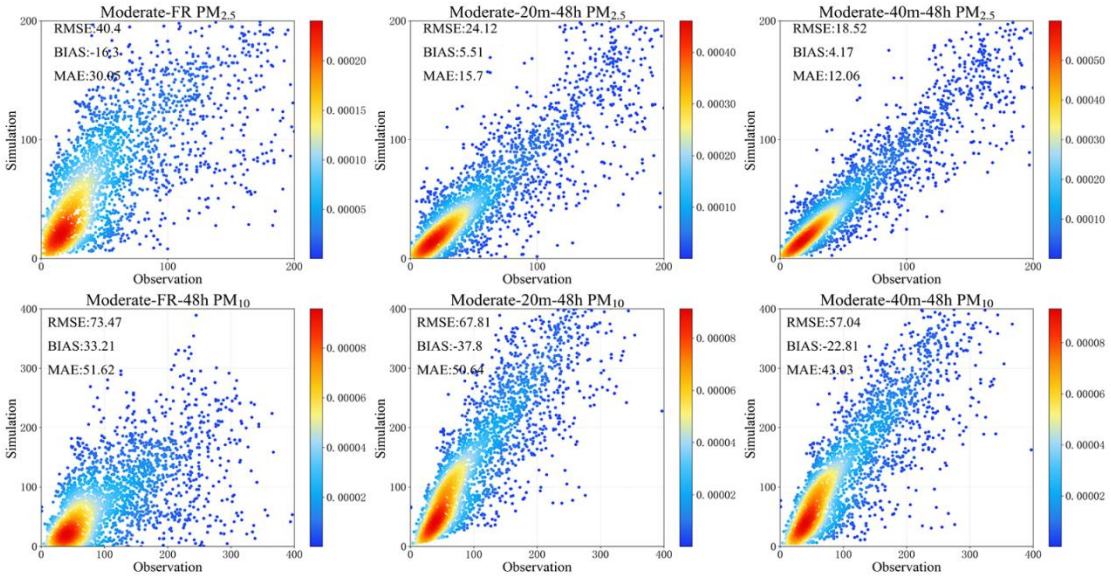

Figure S8. Scatter and density plots of $PM_{2.5}$ and PM_{10} observations from verification stations versus those in Moderate-FR-48h, Moderate-20m-48h and Moderate-40m-48h (units: $\mu g\ m^{-3}$).

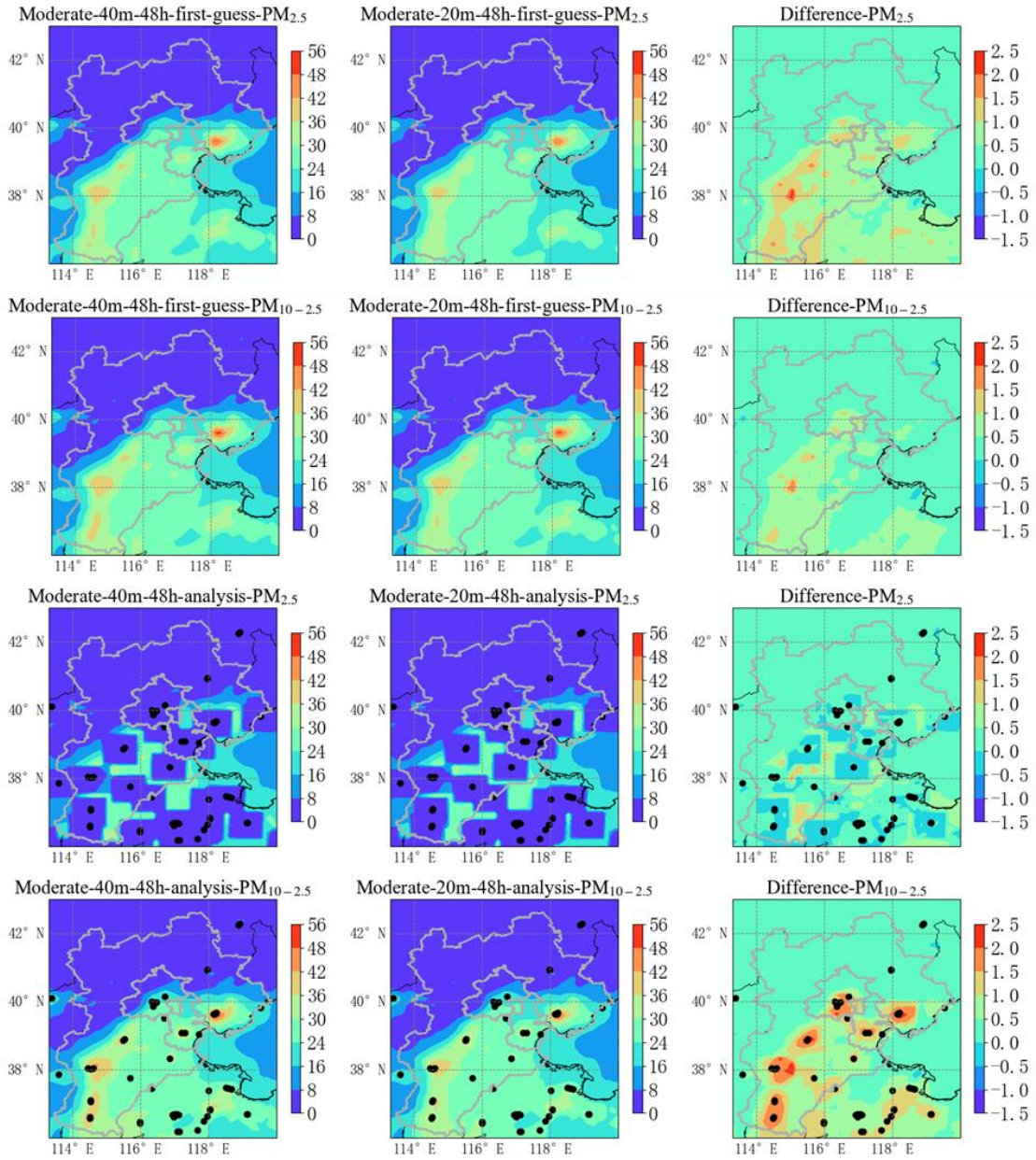

Figure S9. Contour maps of spatial distributions of temporal averaged $PM_{2.5}$ and $PM_{10\text{-}2.5}$ standard deviations in the first guess (first and second row) and analysis (third and fourth row) of Moderate-40m-48h, Moderate-20m-48h and their difference (Moderate-40m-48h minus Moderate-20m-48h) in a moderate haze event (units: μg m^{-3}). The black dots in analysis of $PM_{2.5}$ and $PM_{10\text{-}2.5}$ implies the location of assimilated stations. The grey border implies the BTH region.